

SPATIAL COX PROCESSES IN AN INFINITE-DIMENSIONAL FRAMEWORK

M. P. Frías, A. Torres-Signes and M. Dolores Ruiz-Medina

Abstract

We introduce a new class of spatial Cox processes driven by a Hilbert-valued random log-intensity. We adopt a parametric framework in the spectral domain, to estimate its spatial functional correlation structure. Specifically, we consider a spectral functional, based on the periodogram operator, inspired on Whittle estimation methodology. Strong-consistency of the parametric estimator is proved in the linear case. We illustrate this property in a simulation study under a Gaussian first order Spatial Autoregressive Hilbertian scenario for the log-intensity model. Our method is applied to the spatial functional prediction of respiratory disease mortality in the Spanish Iberian Peninsula, in the period 1980–2015.

Keywords: Infinite-dimensional log-intensity; Periodogram operator; Respiratory disease mortality; Spatial Autoregressive Hilbertian processes; Spatial Cox processes

1 Introduction

Spatial point processes constitute an important branch of stochastic modeling and statistics for countable point sets on a planar space, generated by a random mechanism. These processes are applied in many different fields such as geology, seismology, economics, image processing, ecology, or biology. Particularly, the close relation between point processes and geostatistical data has been largely exploited in the field of spatio-temporal correlation analysis. There exists indeed an extensive literature on statistical modeling and analysis of point processes (see, e.g., [26], [6]; [19]; [8], among others). The reader is referred to [26] and [6], and the references therein, for a theoretical background.

The Poisson process is the most basic and simplest model of point processes. This process can be used to build a more flexible and fundamental class of models, named Cox processes. A Cox process (also called doubly stochastic Poisson process) is obtained as an extension of a Poisson process by considering

the intensity function of a non-homogeneous Poisson process a realization of a random function (i.e., a stochastic process in the one-parameter case, or a random field in the multiparameter case). Cox processes are natural models for point process phenomena that are environmentally driven, but much less natural for phenomena driven primarily by interactions amongst the points (see, e.g., [26]). Cox processes were already introduced and studied in [4] (see also [14] and [34]). An attractive feature of Cox processes is the characterization of its marginal distributions from the higher-order moments of the corresponding random intensity function.

The literature offers several subclasses of Cox processes of particular interest. We call our attention here to log-Gaussian Cox processes (LGCP) (see, e.g., [24]) which are defined as Cox processes with a random intensity being the exponential of a Gaussian stochastic process or random field. The log-normal intensity model provides a flexible framework in spatial and spatio-temporal point pattern analysis (see [10]; [13]). The complete characterization of this process class by the intensity and second order product density makes possible its application in different fields (see, e.g., [29] in pine forest; [32] in wildfire occurrences). Some extensions have also been formulated in [25]; [33]; [38], among others. Our paper goes beyond the real-valued case, by introducing Cox processes driven by a spatial Hilbert-valued (\mathcal{H} -valued) log-intensity random field.

Spatio-temporally indexed data have become more widely available in many scientific fields driving an acceleration of methodological developments. This includes point patterns in space and time (see a review in [13]), real-marked spatial point patterns or multivariate spatial point patterns ([21]; [38]). So far, the literature has focussed on the Euclidean plane, and develops the theoretical tools under this paradigm. In particular, in [38], a multivariate version of log-Gaussian Cox processes is proposed to perform statistical analysis of multivariate point pattern data, whose cross-pair correlation functions are given in the Euclidean space. The pair correlation function is one of most informative second order summary statistics of a spatial point process ([26]; [19]). Kernel-based non-parametric estimation of the pair correlation function is commonly found in the literature ([24]; [13]). Some alternatives exist in a Bayesian framework (see [40]). We also refer to the componentwise approach, based on orthogonal series density estimators of the pair correlation function (see, e.g., [22], where consistency and asymptotic normality is proved).

Kernel estimators are computationally fast but suffer from strong bias for spatial lags close to zero. This is a major drawback if one attempts to infer a parametric model from a non-parametric estimation, given that the behavior near zero is important for determining the right parametric model (see [20]). Thus, parametric estimation should be pursued, particularly, for first and second order moment-based analysis. However, there are not many attempts in this line.

[16] consider pairs of spatial point processes with intensity functions sharing a common multiplicative term, and introduce a conditional likelihood estimation approach to fit a parametric model for the pair correlation function. They establish the consistency of the resulting estimator, and discuss how the parametric estimator can be applied in model diagnostics and inference on regression parameters for the intensity functions. [37] propose parameter estimation for inhomogeneous spatial point processes with a regression model for the intensity function, under tractable second order properties (K -function). Regression parameters are estimated from a Poisson likelihood score function. In a second step, minimum contrast estimation is applied to the residual parameters. Asymptotic normality of parameter estimators is established under certain mixing conditions. The present paper adopts a parametric framework in the spectral domain for the estimation of the spatial functional correlation structure. Specifically, a Whittle-like functional based on the periodogram operator is considered.

Summarizing, a certain imbalance is observed in some methodological branches of the statistics for point processes. However, in general terms, the literature in the field of spatial and spatio-temporal point processes has presented a remarkable growth, in the parametric (likelihood, pseudo-likelihood, composite likelihood), semi-parametric and non-parametric frameworks, and from classical and Bayesian perspectives (see [1]; [15]; [9]; [12], and the references therein).

In a parallel vein, Functional Data Analysis (FDA) techniques are well suited to estimate summary statistics, which are functional in nature. In particular, point process data classification, based on second order statistics, can be performed applying FDA methodologies (see, e.g., pp. 135–150 in [1], and [19]). But FDA is a relatively new branch in point pattern analysis. A functional approach is proposed in [39] to obtain the covariance structure of the random densities, in the case where the shapes of the intensity functions that generate the observed event times are not known. A reconstruction formula is derived for the object-specific density functions to approximate the distribution of event times observed over a fixed time interval. Another attempt, that contributes to the infinite-dimensional counting process framework can be found in [3], where an ℓ^2 -valued homogeneous Poisson process is introduced, addressing parameter estimation and prediction, from classical and Bayesian frameworks. The equivalent asymptotic efficient behavior of both approaches is also proved. In [35], a family of ℓ^2 -valued temporal log-Gaussian Cox processes is introduced. An Autoregressive Hilbertian ($\text{ARH}(1)$) process-based estimation methodology is applied for functional prediction of the Gaussian log-intensity.

This paper introduces a new class of spatial Cox processes, driven by a Hilbert-valued random log-intensity. We consider the weak-sense definition of the functional values of the log-intensity. We refer the resulting generalized log-intensity random field model as the generalized log-risk process. The

conditional marginal probability distributions of the associated counting random measure are Poisson distributed. As usual, in the log–Gaussian case, the spatial functional correlation structure of the random log–intensity characterizes higher order moments. Under stationarity in space, a parametric framework is adopted here in the spatial functional spectral domain. In the spirit of Whittle estimation methodology, second order summary functional statistics are then approximated in terms of a spectral functional, based on the periodogram and spectral density operators. Our loss function measures the proximity of the empirical spatial functional correlation structure of the data, reflected by the periodogram operator, and the elements of the parametric spectral density operator family tested. Strong-consistency of the formulated parametric estimator of the second order product density is proved.

To illustrate our results, a simulation study is undertaken under a Spatial Autoregressive Hilbertian (SARH(1)) process framework (see [30]). We apply our approach to the parametric estimation of the eigenvalues and eigenvectors of the involved autocorrelation operators. These parametric estimators allow the approximation of the spectral density operator. The strong and mean–square consistency are illustrated. Particularly, in the first numerical example, we estimate the hyperparameter defining the support of the eigenvectors of the involved autocorrelation operators. The problem of estimating scale and localization hyperparameters, characterizing the eigenvalues of the autocorrelation operators, is addressed in a second numerical example. Our estimation methodology is also implemented with real–data. Namely, we analyze respiratory disease mortality in the Spanish Iberian Peninsula during the period 1980–2015. The Spanish National Statistical Institute provided the data, consisting of 432 monthly records on respiratory disease mortality at the 48 Spanish provinces.

The outline of the paper is the following. Section 2 introduces the spatial Cox process class, driven by a spatial Hilbert–valued log–intensity. Section 3 derives the strong–consistent parametric estimation of its spatial functional correlation structure in the spectral domain. A simulation study illustrates in Section 4 the properties of the presented spatial functional estimation approach. This approach is validated using real data in Section 5. The paper ends with some final discussion.

2 Cox processes driven by a spatial \mathcal{H} –valued random log–intensity

In what follows, denote by (Ω, \mathcal{A}, P) the probability space over which we define all random variables in this paper. In the subsequent developments, we omit the

dependency on $\omega \in \Omega$ of all measurable mappings, from (Ω, \mathcal{A}, P) to the real or complex line, as well as from (Ω, \mathcal{A}, P) to a function space. We only reflect such dependency the first time, when conditional probability distributions are introduced from the observation of their sample values. Usually, the subindex denotes the location of the element of a given family of operators or random variables, and the argument refers to the element located on the set defining its support.

Let \mathcal{H} be a real separable Hilbert space of functions, and denote by $\mathcal{H} + i\mathcal{H}$ its complex version. In the following, $\langle \cdot, \cdot \rangle$ and $\|\cdot\|$ respectively denote the inner product and norm on the space $\mathcal{H} + i\mathcal{H}$. The same notation will be used for the inner product and norm of \mathcal{H} , considered as a subspace of $\mathcal{H} + i\mathcal{H}$. For practical purposes we refer to $\mathcal{H} = L^2(\mathcal{T})$, the space of square-integrable functions on the time interval \mathcal{T} . In this section, B will stand for a bounded Borel set $B \in \mathcal{B}^d$.

Denote by $\{\varkappa_{\mathbf{z}}, \mathbf{z} \in \mathbb{R}^d\}$ a spatial random process with values in \mathcal{H} . Applying Riesz Representation Theorem, we can define a random functional $X_{\mathbf{z}}$ on \mathcal{H} by the identity

$$X_{\mathbf{z}}(\varphi) = \langle \varkappa_{\mathbf{z}}, \varphi \rangle, \quad \forall \varphi \in \mathcal{H}, \quad \mathbf{z} \in \mathbb{R}^d.$$

From a technical point of view, this definition will help us to introduce different concepts related to the probability distribution, and spatial extrapolation of \mathcal{H} -valued random variables.

Remark 1 *Note that under the assumption*

$$\sum_{p=1}^{\infty} E |\langle \varkappa_{\mathbf{z}}, \phi_p \rangle|^2 = \sum_{p=1}^{\infty} E |X_{\mathbf{z}}(\phi_p)|^2 < \infty, \quad \mathbf{z} \in \mathbb{R}^d, \quad (1)$$

for any orthonormal basis $\{\phi_p, p \geq 1\}$ of \mathcal{H} , $\varkappa_{\mathbf{z}}$ is a random element in \mathcal{H} , i.e., $P[\varkappa_{\mathbf{z}} \in \mathcal{H}] = 1$, for any $\mathbf{z} \in \mathbb{R}^d$ (see [23]). Hence, both identities, strong-sense (pointwise), and weak-sense (as a functional on \mathcal{H}) identities will appear throughout this paper. For example, in equation (2) below the pointwise definition of $\varkappa_{\mathbf{z}} \in \mathcal{H}$ is considered, while in equation (3) its weak-sense definition is applied.

Consider now the spatial functional random intensity $\Lambda = \{\Lambda_{\mathbf{z}}(\cdot), \mathbf{z} \in \mathbb{R}^d\}$ defined as

$$\Lambda_{\mathbf{z}}(t) = \exp(\varkappa_{\mathbf{z}}(t)) = \sum_{k=1}^{\infty} \frac{[\varkappa_{\mathbf{z}}(t)]^k}{k!}, \quad \forall t \in \mathcal{T}, \quad \mathbf{z} \in \mathbb{R}^d, \quad (2)$$

where $\varkappa_{\mathbf{z}}(t)$ denotes the pointwise value of the mapping $t \rightarrow \varkappa_{\mathbf{z}}(t)$, $t \in \mathcal{T}$, since $\varkappa_{\mathbf{z}} \in \mathcal{H} = L^2(\mathcal{T})$, almost surely. Note that $\varkappa_{\mathbf{z}} : (\Omega, \mathcal{A}, P) \rightarrow \mathcal{H}$ defines

a measurable function, for any $\mathbf{z} \in \mathbb{R}^d$. By construction, for a given $\omega \in \Omega$, set $\ln(\lambda_{\mathbf{z}})(t) := \kappa_{\mathbf{z}}(\omega, t) = \mathcal{X}_{\mathbf{z}}(t)$, for every $t \in \mathcal{T}$, and $\mathbf{z} \in \mathbb{R}^d$. The realizations $\boldsymbol{\lambda} = \{\lambda_{\mathbf{z}}(\cdot), \mathbf{z} \in \mathbb{R}^d\}$ of $\boldsymbol{\Lambda} = \{\Lambda_{\mathbf{z}}(\cdot), \mathbf{z} \in \mathbb{R}^d\}$ are then almost surely (a.s.) positive. As commented before, we omit the dependence on $\omega \in \Omega$ of the realizations $\{\kappa_{\mathbf{z}}(\omega, \cdot) = \mathcal{X}_{\mathbf{z}}(\cdot), \mathbf{z} \in \mathbb{R}^d, \omega \in \Omega\}$ of the spatial \mathcal{H} -valued log-intensity $\{\kappa_{\mathbf{z}}, \mathbf{z} \in \mathbb{R}^d\}$.

The following condition is now considered.

Assumption A1. For any $B \in \mathcal{B}^d$, assume

$$\int_B \exp(X_{\mathbf{z}}(\varphi)) d\mathbf{z} = \int_B \exp(\langle \kappa_{\mathbf{z}}, \varphi \rangle) d\mathbf{z} < \infty, \quad \forall \varphi \in \mathcal{H}, \quad (3)$$

in the norm of the space $\mathcal{L}^2(\Omega, \mathcal{A}, P)$, given by $\|X\|_{\mathcal{L}^2(\Omega, \mathcal{A}, P)}^2 = E[X^2]$, for any zero-mean second order random variable X on (Ω, \mathcal{A}, P) .

Remark 2 From **Assumption A1**, the marginal probability distributions of the introduced Cox process family have finite second order moments. Equation (3) holds if the process $\{\kappa_{\mathbf{z}}(t), t \in \mathcal{T}, \mathbf{z} \in \mathbb{R}^d\}$ is continuous in the mean-square sense with respect to both arguments $t \in \mathcal{T}$, and $\mathbf{z} \in \mathbb{R}^d$, which is equivalent to assume that the kernel $r_{\mathbf{z}, \mathbf{y}}(t, s) = E[\kappa_{\mathbf{z}}(t)\kappa_{\mathbf{y}}(s)]$, defining the covariance operator $\mathcal{R}_{\mathbf{z}, \mathbf{y}} = E[\kappa_{\mathbf{z}} \otimes \kappa_{\mathbf{y}}]$ is continuous in $t, s \in \mathcal{T}$, and $\mathbf{z}, \mathbf{y} \in \mathbb{R}^d$. Here, $\kappa_{\mathbf{z}} \otimes \kappa_{\mathbf{y}}$ denotes the tensorial product of two random elements in \mathcal{H} . Hence, it defines a Hilbert-Schmidt operator on \mathcal{H} almost surely.

Let now $N : (\Omega, \mathcal{A}, \mathcal{P}) \times \mathcal{B}^d \rightarrow \mathbb{N}$ be a random counting measure over the Borel σ -algebra \mathcal{B}^d of \mathbb{R}^d . That is, for each $\omega \in \Omega$ fixed, $N(\omega, B)$, $B \in \mathcal{B}^d$, defines a counting measure on the sets of \mathcal{B}^d , while, for each set $B \in \mathcal{B}^d$, $N(\omega, B)$, $\omega \in \Omega$, defines a integer-valued random variable on (Ω, \mathcal{A}, P) . We assume that, for any $\varphi \in \mathcal{H}$, the conditional probability distribution of the number $N(B)$ of random events that occur on a set B , given the spatial realization $x(\varphi) = \{x_{\mathbf{z}}(\varphi) = \langle \mathcal{X}_{\mathbf{z}}, \varphi \rangle, \mathbf{z} \in \mathbb{R}^d\}$ of $X(\varphi)$, follows a Poisson probability distribution with mean $\int_B \exp(x_{\mathbf{z}}(\varphi)) d\mathbf{z}$, for any $B \in \mathcal{B}^d$. Here, as before, for every $\varphi \in \mathcal{H}$, $x(\varphi) = \{x_{\mathbf{z}}(\varphi) = \langle \mathcal{X}_{\mathbf{z}}, \varphi \rangle, \mathbf{z} \in \mathbb{R}^d\}$ is computed from the sample curves $\mathcal{X}_{\mathbf{z}} \in \mathcal{H}$, spatially distributed over $\mathbf{z} \in \mathbb{R}^d$.

Remark 3 We consider the terminology test function in a wide sense from Riesz Representation Theorem. Note that FDA techniques are usually applied after interpolation and smoothing of the data. Local singular behaviors are then regularized. Alternatively, when high-singular systems are analyzed, the space $C_0^\infty(\mathcal{T})$ of infinitely differentiable functions with compact support in \mathcal{T} is usually considered as test function space, allowing the regularization of the system.

2.1 Least-squares prediction and marginal second order moments

We introduce the first and second order moments of the marginal conditional probability distributions of our random measure $\{N(B); |B| < \infty, B \in \mathcal{B}^d\}$, where $|B| = \int_B d\mathbf{z}$.

For $B \in \mathcal{B}^d$ and $\varphi \in \mathcal{H}$, the conditional Poisson probability distribution of $N(B)$, given $x_{\mathbf{z}}(\varphi)$, $\mathbf{z} \in \mathbb{R}^d$, leads to

$$\begin{aligned} f_{N(B)/x_{\mathbf{z}}(\varphi), \mathbf{z} \in \mathbb{R}^d}(t) &:= E [\exp(tN(B)) / x_{\mathbf{z}}(\varphi), \mathbf{z} \in \mathbb{R}^d] \\ &= \exp \left(\left[\int_B \exp(x_{\mathbf{z}}(\varphi)) d\mathbf{z} \right] (\exp(t) - 1) \right), \quad t \in \mathbb{R}, \quad \forall \varphi \in \mathcal{H}. \end{aligned} \quad (4)$$

As usual, the least-squares predictor $\widehat{N(B)}$ of $N(B)$ is computed from the first derivative of (4) at $t = 0$. Thus,

$$\widehat{N(B)} = E [N(B) / x_{\mathbf{z}}(\varphi), \mathbf{z} \in \mathbb{R}^d] = \int_B \exp(x_{\mathbf{z}}(\varphi)) d\mathbf{z}, \quad (5)$$

which coincides with the conditional variance. The corresponding variance decomposition formula is computed from the following identities, obtained from the second derivative of (4) at $t = 0$

$$\begin{aligned} E [\text{Var} (N(B) / X_{\mathbf{z}}(\varphi), \mathbf{z} \in \mathbb{R}^d)] &= \int_B E [\exp(X_{\mathbf{z}}(\varphi))] d\mathbf{z} \\ \text{Var} (E [N(B) / X_{\mathbf{z}}(\varphi), \mathbf{z} \in \mathbb{R}^d]) &= \int_{B \times B} E [\exp(X_{\mathbf{z}}(\varphi) + X_{\mathbf{y}}(\varphi))] d\mathbf{z} d\mathbf{y} \\ &\quad - \int_{B \times B} E [\exp(X_{\mathbf{z}}(\varphi))] E [\exp(X_{\mathbf{y}}(\varphi))] d\mathbf{z} d\mathbf{y}, \end{aligned} \quad (6)$$

where from (5)

$$E_{\varphi} [N(B)] = \int_B E [\exp(X_{\mathbf{z}}(\varphi))] d\mathbf{z}, \quad (7)$$

for $B \in \mathcal{B}^d$ and for any $\varphi \in \mathcal{H}$. Thus, from (6) and (7), we obtain

$$\begin{aligned} \text{Var}_{\varphi} (N(B)) &= \int_B E [\exp(X_{\mathbf{z}}(\varphi))] d\mathbf{z} \\ &\quad + \int_{B \times B} E [\exp(X_{\mathbf{y}}(\varphi) + X_{\mathbf{z}}(\varphi))] d\mathbf{y} d\mathbf{z} \\ &\quad - \int_{B \times B} E [\exp(X_{\mathbf{y}}(\varphi))] E [\exp(X_{\mathbf{z}}(\varphi))] d\mathbf{y} d\mathbf{z}. \end{aligned} \quad (8)$$

In the spatial stationary log-Gaussian case, equations (7)–(8) can be rewritten in terms of the second order moments of a zero-mean Gaussian spatial \mathcal{H} -valued log-intensity $\{\varkappa_{\mathbf{z}}, \mathbf{z} \in \mathbb{R}^d\}$. For every $\varphi \in \mathcal{H}$ and set $B \in \mathcal{B}^d$,

$$\begin{aligned} E_{\varphi}[N(B)] &= \exp\left(\frac{\mathcal{R}_0(\varphi)(\varphi)}{2}\right) |B| \\ \text{Var}_{\varphi}(N(B)) &= \exp(\mathcal{R}_0(\varphi)(\varphi)) \int_{B \times B} \exp\left(\frac{\mathcal{R}_{\mathbf{z}-\mathbf{y}}(\varphi)(\varphi) + \mathcal{R}_{\mathbf{y}-\mathbf{z}}(\varphi)(\varphi)}{2}\right) d\mathbf{z} d\mathbf{y} \\ &\quad + |B| \exp\left(\frac{\mathcal{R}_0(\varphi)(\varphi)}{2}\right) \left[1 - |B| \exp\left(\frac{\mathcal{R}_0(\varphi)(\varphi)}{2}\right)\right], \end{aligned} \quad (9)$$

where, as before, $|B|$ denotes the Lebesgue measure of B , and $\mathcal{R}_{\mathbf{z}-\mathbf{y}}$ is the spatial covariance operator of $\{\varkappa_{\mathbf{z}}, \mathbf{z} \in \mathbb{R}^d\}$ given by

$$\begin{aligned} \mathcal{R}_{\mathbf{z}-\mathbf{y}}(f)(g) &= E \langle X_{\mathbf{z}} \otimes X_{\mathbf{y}}(f), g \rangle = E [X_{\mathbf{z}}(g) X_{\mathbf{y}}(f)] \\ &= E [\langle \varkappa_{\mathbf{z}}, g \rangle \langle \varkappa_{\mathbf{y}}, f \rangle], \quad \forall f, g \in \mathcal{H}, \quad \mathbf{z}, \mathbf{y} \in \mathbb{R}^d. \end{aligned} \quad (10)$$

The n -order product density is then computed from the intensity and second order product density as follows. For $\varphi \in \mathcal{H}$,

$$\begin{aligned} \rho_{\varphi}^{(n)}(\mathbf{z}_1, \dots, \mathbf{z}_n) &= E \left[\prod_{i=1}^n \exp(x_{\mathbf{z}_i}(\varphi)) \right] = E \left[\exp\left(\sum_{i=1}^n x_{\mathbf{z}_i}(\varphi)\right) \right] \\ &= [\rho_{\varphi}]^n \exp\left(\frac{1}{2} \sum_{i=1}^n \sum_{j=1}^n \mathcal{R}_{\mathbf{z}_i-\mathbf{z}_j}(\varphi)(\varphi)\right), \quad \mathbf{z}_1, \dots, \mathbf{z}_n \in \mathbb{R}^d, \end{aligned} \quad (11)$$

with the spatial functional intensity ρ_{φ} defined as

$$\rho_{\varphi} = \rho_{\varphi}^{(1)}(\mathbf{z}) = \exp\left(\frac{\mathcal{R}_0(\varphi)(\varphi)}{2}\right), \quad \forall \mathbf{z} \in \mathbb{R}^d, \quad \varphi \in \mathcal{H}. \quad (12)$$

In the isotropic case, for $i, j = 1, \dots, n$, the spatial pair correlation functional is defined from the identity

$$g_{\varphi}(\mathbf{z}_j - \mathbf{z}_i) = \frac{\rho_{\varphi}^{(2)}(\mathbf{z}_i - \mathbf{z}_j)}{[\rho_{\varphi}]^2} = \exp(\mathcal{R}_{\mathbf{z}_i-\mathbf{z}_j}(\varphi)(\varphi)), \quad \forall \varphi \in \mathcal{H}. \quad (13)$$

3 Strong-consistent estimation of the spatial functional correlation structure of the log-intensity

We propose a strong-consistent parametric estimator of the spectral density operator, inspired on the Whittle functional (see [28] in the nonparametric framework). We restrict our attention here to the case $\{\kappa_{\mathbf{z}}, \mathbf{z} \in \mathbb{Z}^d\}$, i.e., the \mathcal{H} -valued log-intensity is observed on a spatial regular grid. We then consider the interval $[-\pi, \pi]^d$ as the index set of our spectral density operator family $\{\mathcal{F}_{\xi}, \xi \in [-\pi, \pi]^d\}$, given by

$$\mathcal{F}_{\xi}(h)(g) = \frac{1}{(2\pi)^d} \sum_{\mathbf{z} \in \mathbb{Z}^d} \exp\left(-i \sum_{j=1}^d \xi_j z_j\right) \mathcal{R}_{\mathbf{z}}(h)(g), \quad \xi \in [-\pi, \pi]^d, \quad (14)$$

for all $h, g \in \mathcal{H} + i\mathcal{H}$. We assume the series $\frac{1}{(2\pi)^d} \sum_{\mathbf{z} \in \mathbb{Z}^d} \exp\left(-i \sum_{j=1}^d \xi_j z_j\right) \mathcal{R}_{\mathbf{z}}$ converges in the trace norm (see, e.g., [28]), where, for any $\mathbf{z} \in \mathbb{R}^d$, the covariance operator $\mathcal{R}_{\mathbf{z}}$ has been introduced in (10).

We assume the following condition.

Assumption A2. Let $\mathbf{z} = (z_1, \dots, z_d) \in \mathbb{Z}^d$, with $z_i \in [-\mathcal{N}_i + 1, \mathcal{N}_i - 1]$, $i = 1, \dots, d$, and $\mathcal{N} = \mathcal{N}_1 \times \dots \times \mathcal{N}_d$. For an orthonormal basis $\{\psi_k, k \geq 1\}$ of \mathcal{H} , assume that as $\mathcal{N} \rightarrow \infty$,

$$\sum_{k, l \geq 1} \left\| \left[\frac{1}{\mathcal{N}} \left[\sum_{y_1=1}^{\mathcal{N}_1-z_1} \dots \sum_{y_d=1}^{\mathcal{N}_d-z_d} X_{\mathbf{y}}(\psi_k) X_{\mathbf{y}+\mathbf{z}}(\psi_l) \right] - \mathcal{R}_{\mathbf{z}}(\psi_k)(\psi_l) \right] \right\|^2 \rightarrow \text{a.s. } 0,$$

where we have used the notation $\mathbf{y} = (y_1, \dots, y_d) \in \prod_{i=1}^d [1, \mathcal{N}_i - z_i] \cap \mathbb{Z}^d$.

This condition provides the ergodicity, in the second order moment sense, with respect to the Hilbert-Schmidt operator norm $\|\cdot\|_{\mathcal{S}(\mathcal{H})}$ of the spatial functional log-intensity process $\{\kappa_{\mathbf{z}}, \mathbf{z} \in \mathbb{Z}^d\}$.

Remark 4 As usual, strong-consistency in the \mathcal{H} -valued context is defined from the a.s. convergence in the norm $\|\cdot\|_{\mathcal{H}}$. This fact is applied in **Assumption A2**, considering the Hilbert space $\mathcal{S}(\mathcal{H})$ of Hilbert-Schmidt operators on \mathcal{H} . Thus **Assumption A2** defines the strong-consistency of the empirical functional second order moments of $\kappa_{\mathbf{z}}$ with respect to $\mathcal{S}(\mathcal{H})$ -norm.

Remark 5 **Assumption A2** is satisfied, in particular, when

$$\sum_{\mathbf{z} \in \mathbb{Z}^d} \|\mathcal{R}_{\mathbf{z}}\|_{L^1(\mathcal{H})} < \infty,$$

with, for $\mathbf{z} \in \mathbb{R}^d$, $\|\mathcal{R}_{\mathbf{z}}\|_{L^1(\mathcal{H})} = \sum_{k \geq 1} \langle [\mathcal{R}_{\mathbf{z}}^* \mathcal{R}_{\mathbf{z}}]^{1/2}(\varphi_k), \varphi_k \rangle$, for any orthonormal basis $\{\varphi_k, k \geq 1\}$ of \mathcal{H} (see Corollary 2.3 in [2]). Under this condition, the spectral density operator \mathcal{F}_{ξ} is a nuclear operator for any $\xi \in [-\pi, \pi]^d$.

Consider now a parametric family of spectral density operators

$$\{\mathcal{F}_{\xi, \theta}, \xi \in [-\pi, \pi]^d, \theta \in \Theta \subset \mathbb{R}^q\},$$

where the compact parameter space $\Theta \subset \mathbb{R}^q$, $q \geq 1$, is such that

$$\left\| \int_{[-\pi, \pi]^d} \mathcal{F}_{\xi, \theta_1} \mathcal{F}_{\xi, \theta_2}^{-1} d\xi \right\|_{\mathcal{L}(\mathcal{H} + i\mathcal{H})} = \left\| \int_{[-\pi, \pi]^d} \mathcal{F}_{\xi, \theta_2}^{-1} \mathcal{F}_{\xi, \theta_1} d\xi \right\|_{\mathcal{L}(\mathcal{H} + i\mathcal{H})} < \infty, \quad (15)$$

for every $\theta_1, \theta_2 \in \Theta$. Here, $\|\cdot\|_{\mathcal{L}(\mathcal{H} + i\mathcal{H})}$ denotes the norm in the space of bounded linear operators on $\mathcal{H} + i\mathcal{H}$.

Note that Examples 1 and 2 in Section 4 provide a suitable scenario where condition (15) is satisfied in the functional linear setting. Specifically, in the one-parameter scenario of Example 1, θ characterizes the support of the eigenvectors of the autocorrelation operators. In Example 2, the components of θ are location and scale parameters involved in the definition of the parameterized eigenvalues of the autocorrelation operators. Particularly, the presented approach extends to the infinite-dimensional framework the parametric linear modeling adopted in [17] in the real-valued case.

The following four assumptions are considered in the functional linear parametric framework adopted in Theorem 1 below. For an arbitrary orthonormal basis $\{\varphi_k, k \geq 1\}$ of $\mathcal{H} + i\mathcal{H}$ assume:

(C1) For $\theta, \theta' \in \Theta$, with $\theta \neq \theta'$, the set $\{\xi \in [-\pi, \pi]^d; \mathcal{F}_{\xi, \theta} \neq \mathcal{F}_{\xi, \theta'}\}$ has positive Lebesgue measure. Hence, different θ values correspond to different spatial functional dependence structures.

(C2) Operator $\mathcal{F}_{\xi, \theta}$ is continuous over $\xi \in [-\pi, \pi]^d$, and $\theta \in \Theta$, with respect to $\mathcal{L}(\mathcal{H} + i\mathcal{H})$ -norm. That is, $\|\mathcal{F}_{\xi, \theta} - \mathcal{F}_{\xi^*, \theta^*}\|_{\mathcal{L}(\mathcal{H} + i\mathcal{H})} \rightarrow 0$, $(\xi, \theta) \rightarrow (\xi^*, \theta^*)$, for all $(\xi^*, \theta^*) \in [-\pi, \pi]^d \times \Theta$.

(C3) The spatial functional infinite-order moving average representation of the log-intensity process is given in terms of a generalized \mathcal{H} -valued white noise innovation process having identity autocovariance operator. Thus,

$$\int_{[-\pi, \pi]^d} \log((2\pi)^d \mathcal{F}_{\xi, \theta}(\varphi_k)(\varphi_k)) d\xi = 0, \quad \forall k \geq 1, \theta \in \Theta. \quad (16)$$

(C4) The Cesaro sum of the Fourier series of $\mathcal{F}_{\xi, \theta}^{-1}(\varphi_k)(\varphi_k)$ converges uniformly in $\xi \in [-\pi, \pi]^d$, $k \geq 1$, and $\theta \in \Theta$.

Remark 6 In the functional linear time series setting, the \mathcal{H} -valued innovation process has usually trace autocovariance operator (see, e.g., [2]). Under (C3), we have introduced a more general framework for such innovation process, defined by a generalized random field model with identity autocovariance operator.

Remark 7 As pointed out in Remark 6, the projections of the innovation process onto an orthonormal basis of \mathcal{H} define a spatial white noise process with unit variance. This local singular behavior displayed by our generalized innovation random field model is regularized by convolution with a suitable linear operator sequence. Thus, the spatial summability of the square of the Hilbert–Schmidt operator norm of this sequence should be assumed. This condition is equivalent to the integrability in the frequency domain of the trace norm of the spectral density operator.

Let $\tilde{\kappa}_{\xi}^{\mathcal{N}}$ be the functional discrete Fourier transform of the data, given by the following identity in the norm of $\mathcal{H} + i\mathcal{H}$,

$$\tilde{\kappa}_{\xi}^{\mathcal{N}} = \frac{1}{\sqrt{\mathcal{N}(2\pi)^d}} \sum_{y_1=1}^{\mathcal{N}_1} \cdots \sum_{y_d=1}^{\mathcal{N}_d} \exp\left(-i \sum_{j=1}^d \xi_j y_j\right) \kappa_{\mathbf{y}}, \quad \xi \in [-\pi, \pi]^d, \quad \mathcal{N} = \prod_{i=1}^d \mathcal{N}_i, \quad (17)$$

where we have applied that $\tilde{\kappa}_{\xi}^{\mathcal{N}} \in \mathcal{H} + i\mathcal{H}$, almost surely, for any $\xi \in [-\pi, \pi]^d$, in view of the trace property of the autocovariance operator of $\{\kappa_{\mathbf{z}}, \mathbf{z} \in \mathbb{R}^d\}$ (see equation (1) in Remark 1). The periodogram operator is then defined as the empirical operator

$$\begin{aligned} \mathcal{I}_{\xi}^{\mathcal{N}}(g)(h) &= \frac{1}{\mathcal{N}(2\pi^d)} \sum_{y_1=1}^{\mathcal{N}_1} \cdots \sum_{y_d=1}^{\mathcal{N}_d} \sum_{z_1=1}^{\mathcal{N}_1} \cdots \sum_{z_d=1}^{\mathcal{N}_d} X_{y_1, \dots, y_d}^{\mathcal{N}}(h) \\ &\quad \times X_{z_1, \dots, z_d}^{\mathcal{N}}(g) \exp\left(-i \sum_{j=1}^d \xi_j (y_j - z_j)\right), \end{aligned} \quad (18)$$

for $g, h \in \mathcal{H} + i\mathcal{H}$, and $\xi \in [-\pi, \pi]^d$. Note that from (17), the trace property of $\mathcal{I}_{\xi}^{\mathcal{N}}$ follows straightforward from Parseval identity in $\mathcal{H} + i\mathcal{H}$, keeping in mind that $\mathcal{I}_{\xi}^{\mathcal{N}}$ is nonnegative. Under **Assumption A2**, and the above formulated conditions, the following parameter estimator is considered, based on a functional sample size \mathcal{N} ,

$$\hat{\theta}_{\mathcal{N}} = \arg \min_{\theta \in \Theta} [\sigma_{\mathcal{N}}(\theta)], \quad (19)$$

where $\sigma_{\mathcal{N}}(\theta)$ denotes the empirical loss function

$$\begin{aligned}\sigma_{\mathcal{N}}(\theta) &= \sup_{k \geq 1} \frac{1}{(2\pi)^d} \int_{[-\pi, \pi]^d} |\mathcal{F}_{\xi, \theta}^{-1} \mathcal{I}_{\xi}^{\mathcal{N}}(\varphi_k)(\varphi_k)| d\xi \\ &= \sup_{k \geq 1} \frac{1}{(2\pi)^d} \int_{[-\pi, \pi]^d} |\mathcal{I}_{\xi}^{\mathcal{N}} \mathcal{F}_{\xi, \theta}^{-1}(\varphi_k)(\varphi_k)| d\xi, \quad \forall \theta \in \Theta, \quad (20)\end{aligned}$$

whose asymptotic properties will be analyzed in Theorem 1 below.

We consider the corresponding parametric estimator of the spatial covariance operator

$$\widehat{\mathcal{R}}_{\mathbf{z}, \theta}(h)(g) = \frac{1}{(2\pi)^d} \int_{[-\pi, \pi]^d} \exp\left(i \sum_{j=1}^d z_j \xi_j\right) \mathcal{F}_{\xi, \widehat{\theta}_{\mathcal{N}}}(h)(g) d\xi \quad (21)$$

for $h, g \in \mathcal{H}$, and $\mathbf{z} \in \mathbb{Z}^d$. Also, in the isotropic log-Gaussian case, the following parametric estimator of the pair correlation function is obtained

$$\widehat{g}_{\varphi, \theta}(\mathbf{z}) = \exp\left(\widehat{\mathcal{R}}_{\mathbf{z}, \theta}(\varphi)(\varphi)\right) = \exp\left(\mathcal{R}_{\mathbf{z}, \widehat{\theta}_{\mathcal{N}}}(\varphi)(\varphi)\right), \quad \forall \varphi \in \mathcal{H}, \quad \mathbf{z} \in \mathbb{R}^d.$$

In this line of thinking, and though the next result is derived beyond the log-Gaussian assumption, recall that, under the log-Gaussian Cox scenario, the strong-consistency proved in Theorem 1 also holds for the parametric estimator of the product density

$$\rho_{\varphi, \widehat{\theta}_{\mathcal{N}}}^{(n)}(\mathbf{z}_1, \dots, \mathbf{z}_n) = [\rho_{\varphi, \widehat{\theta}_{\mathcal{N}}}]^n \exp\left(\frac{1}{2} \sum_{i=1}^n \sum_{j=1}^n \mathcal{R}_{\mathbf{z}_i - \mathbf{z}_j, \widehat{\theta}_{\mathcal{N}}}(\varphi)(\varphi)\right),$$

for $\mathbf{z}_1, \dots, \mathbf{z}_n \in \mathbb{Z}^d$, and $\varphi \in \mathcal{H}$, with

$$\rho_{\varphi, \widehat{\theta}_{\mathcal{N}}} = \widehat{\rho}_{\varphi, \theta} = \widehat{\rho}_{\varphi, \theta}^{(1)}(\mathbf{z}) = \exp\left(\frac{\mathcal{R}_{\mathbf{0}, \widehat{\theta}_{\mathcal{N}}}(\varphi)(\varphi)}{2}\right), \quad \forall \mathbf{z} \in \mathbb{Z}^d. \quad (22)$$

Theorem 1 *Let $\{\kappa_{\mathbf{z}}, \mathbf{z} \in \mathbb{Z}^d\}$ be a spatial stationary zero-mean \mathcal{H} -valued linear log-intensity random field. Let θ_0 be the true parameter value lying in the interior $\text{Int}(\Theta)$ of Θ . Under **Assumptions A1–A2**, and conditions (15) and (C1)–(C4), the estimator (19)–(20) satisfies*

$$\widehat{\theta}_{\mathcal{N}} \rightarrow_{a.s.} \theta_0, \quad \mathcal{N} \rightarrow \infty, \quad (23)$$

where $\rightarrow_{a.s.}$ means the almost surely convergence.

Proof. We consider here a compact version of the proof. Some additional technical details can be found in the Appendix. Specifically, the proof of this result follows from **Assumption A2** that implies, for any orthonormal basis $\{\varphi_k, k \geq 1\}$ of $\mathcal{H} + i\mathcal{H}$, and for $\mathbf{z} = (z_1, \dots, z_d) \in \mathbb{Z}^d$ with $z_i \in [-\mathcal{N}_i + 1, \mathcal{N}_i - 1]$, $i = 1, \dots, d$,

$$\sum_{k, l \geq 1} |\mathcal{C}(\mathbf{z}, k, l) - \mathcal{R}_{\mathbf{z}, \theta_0}(\varphi_k)(\varphi_l)|^2 \xrightarrow{\text{a.s.}} 0, \quad \mathcal{N} \rightarrow \infty, \quad (24)$$

where the empirical Fourier coefficients $\mathcal{C}(\mathbf{z}, k, l)$ of the periodogram operator are given by

$$\begin{aligned} \mathcal{C}(\mathbf{z}, k, l) &= \int_{[-\pi, \pi]^d} \exp\left(i \sum_{j=1}^d \xi_j z_j\right) \tilde{X}_{\xi}^{\mathcal{N}}(\varphi_k) \tilde{X}_{-\xi}^{\mathcal{N}}(\varphi_l) d\xi \\ &= \frac{1}{\mathcal{N}} \left[\sum_{y_1=1}^{\mathcal{N}_1-z_1} \cdots \sum_{y_d=1}^{\mathcal{N}_d-z_d} X_{\mathbf{y}}(\varphi_k) X_{\mathbf{y}+\mathbf{z}}(\varphi_l) \right], \quad |z_i| < \mathcal{N}_i, \quad i \in \{1, \dots, d\} \\ \mathcal{C}(\mathbf{z}, k, l) &= 0, \quad |z_i| \geq \mathcal{N}_i, \quad \text{for some } i \in \{1, \dots, d\}, \end{aligned} \quad (25)$$

for $\mathbf{y} = (y_1, \dots, y_d) \in \prod_{i=1}^d [1, \mathcal{N}_i - z_i] \cap \mathbb{Z}^d$. Here, $\tilde{X}_{\xi}^{\mathcal{N}}(\varphi) = \langle \tilde{\mathcal{X}}_{\xi}^{\mathcal{N}}, \varphi \rangle$, for every $\varphi \in \mathcal{H} + i\mathcal{H}$.

Let $M = \prod_{j=1}^d M_j$, under (C4), as $M \rightarrow \infty$, the convergence of

$$\begin{aligned} q_{\xi, \theta}^M(\varphi_k)(\varphi_k) &= \frac{1}{(2\pi)^d} \sum_{z_j \in [-M_j+1, M_j-1]; j=1, \dots, d} \exp\left(-i \sum_{j=1}^d \xi_j z_j\right) \\ &\quad \times \prod_{j=1}^d \left(1 - \frac{z_j}{M_j}\right) g(z_1, \dots, z_d, \theta, k) \end{aligned} \quad (26)$$

to $\mathcal{F}_{\xi, \theta}^{-1}(\varphi_k)(\varphi_k)$ holds uniformly in $k \geq 1$, $\xi \in [-\pi, \pi]^d$, and $\theta \in \Theta$. For each $\mathbf{z} = (z_1, \dots, z_d) \in \prod_{j=1}^d [-M_j + 1, M_j - 1]$, $g(\mathbf{z}, \theta, k) = g(z_1, \dots, z_d, \theta, k)$ denotes the \mathbf{z} th-Fourier coefficient of $\mathcal{F}_{\varpi, \theta}^{-1}(\varphi_k)(\varphi_k)$ (see equation (43) in the Appendix).

For M sufficiently large, applying Hölder inequality, **Assumption A2** and conditions (C1)–(C4) lead to the a.s. convergence to zero, as $\mathcal{N} \rightarrow \infty$, for any

$\theta \in \Theta$, of

$$\begin{aligned}
& \lim_{\mathcal{N} \rightarrow \infty} \sup_{k \geq 1} \int_{[-\pi, \pi]^d} \left| q_{\xi, \theta}^M \left[\mathcal{I}_{\xi}^{(\mathcal{N})}(\varphi_k)(\varphi_k) - \mathcal{F}_{\xi, \theta_0}(\varphi_k)(\varphi_k) \right] \right| d\xi \\
& \leq_{a.s.} \lim_{\mathcal{N} \rightarrow \infty} \sup_{k \geq 1} \int_{[-\pi, \pi]^d} \left| q_{\xi, \theta}^M \left[\mathcal{I}_{\xi}^{(\mathcal{N})}(\varphi_k)(\varphi_k) - \mathcal{F}_{\xi, \theta_0}(\varphi_k)(\varphi_k) \right] \right|^2 d\xi \\
& = \lim_{\mathcal{N} \rightarrow \infty} \sup_{k \geq 1} \frac{(2\pi)^d}{\mathcal{N}} \sum_{\mathbf{z}} \left| q_{\xi_{\mathbf{z}}, \theta}^M \mathcal{I}_{\xi_{\mathbf{z}}}^{(\mathcal{N})}(\varphi_k)(\varphi_k) - q_{\xi_{\mathbf{z}}, \theta}^M \mathcal{F}_{\xi_{\mathbf{z}}, \theta_0}(\varphi_k)(\varphi_k) \right|^2 \stackrel{a.s.}{=} 0 \quad (27)
\end{aligned}$$

(see [17], and the Appendix for more details). Applying triangle inequality, under conditions (C3)–(C4),

$$\begin{aligned}
& \sup_{k \geq 1} \int_{[-\pi, \pi]^d} \left| \mathcal{I}_{\xi}^{(\mathcal{N})} \mathcal{F}_{\xi, \theta}^{-1}(\varphi_k)(\varphi_k) - \mathcal{F}_{\xi, \theta_0} \mathcal{F}_{\xi, \theta}^{-1}(\varphi_k)(\varphi_k) \right| d\xi \\
& \leq_{a.s.} \sup_{k \geq 1} \int_{[-\pi, \pi]^d} \left| \mathcal{I}_{\xi}^{(\mathcal{N})} \left[\mathcal{F}_{\xi, \theta}^{-1}(\varphi_k)(\varphi_k) - q_{\xi, \theta}^M(\varphi_k)(\varphi_k) \right] \right| d\xi \\
& + \sup_{k \geq 1} \int_{[-\pi, \pi]^d} \left| q_{\xi, \theta}^M \left[\mathcal{I}_{\xi}^{(\mathcal{N})}(\varphi_k)(\varphi_k) - \mathcal{F}_{\xi, \theta_0}(\varphi_k)(\varphi_k) \right] \right| d\xi \\
& + \sup_{k \geq 1} \int_{[-\pi, \pi]^d} \left| \mathcal{F}_{\xi, \theta_0} \left[q_{\xi, \theta}^M(\varphi_k)(\varphi_k) - \mathcal{F}_{\xi, \theta}^{-1}(\varphi_k)(\varphi_k) \right] \right| d\xi \\
& \leq_{a.s.} [2\pi]^d \varepsilon(M) \sup_{k \geq 1} \mathcal{C}(0, k, k) \\
& + \sup_{k \geq 1} \int_{[-\pi, \pi]^d} \left| q_{\xi, \theta}^M \left[\mathcal{I}_{\xi}^{(\mathcal{N})}(\varphi_k)(\varphi_k) - \mathcal{F}_{\xi, \theta_0}(\varphi_k)(\varphi_k) \right] \right| d\xi \\
& + \varepsilon(M) \sup_{k \geq 1} \mathcal{R}_{0, \theta_0}(\varphi_k)(\varphi_k) \\
& = S_1(\mathcal{N}, M) + S_2(\mathcal{N}, M) + S_3(M), \quad \theta \in \Theta, \quad (28)
\end{aligned}$$

with parameter M denoting, as before, the number of terms involved in the partial Cesaro sum of the Fourier series of $\mathcal{F}_{\xi, \theta}^{-1}$, and $\varepsilon(M)$ being the corresponding residual term. Note that, under (C4), the Fourier series of $\mathcal{F}_{\xi, \theta}^{-1}$ is Cesaro summable in $\mathcal{L}(\mathcal{H} + i\mathcal{H})$ -norm, uniformly in $(\xi, \theta) \in [-\pi, \pi]^d \times \Theta$.

As $\mathcal{N} \rightarrow \infty$, applying a.s. convergence to zero of equation (27),

$$S_2(\mathcal{N}, M) = \sup_{k \geq 1} \int_{[-\pi, \pi]^d} \left| q_{\xi, \theta}^M \left[\mathcal{I}_{\xi}^{(\mathcal{N})}(\varphi_k)(\varphi_k) - \mathcal{F}_{\xi, \theta_0}(\varphi_k)(\varphi_k) \right] \right| d\xi \rightarrow_{a.s.} 0.$$

The Cesaro summability of the Fourier series of $\mathcal{F}_{\xi, \theta}^{-1}$ in $\mathcal{L}(\mathcal{H} + i\mathcal{H})$ -norm, uniformly in $(\xi, \theta) \in [-\pi, \pi]^d \times \Theta$ in (C4) implies that, as $M \rightarrow \infty$, $\varepsilon(M) \rightarrow 0$.

Finally, under **Assumption A2**, $\sup_{k \geq 1} \mathcal{C}(0, k, k) \rightarrow \sup_{k \geq 1} \mathcal{R}_{\mathbf{0}, \theta_0}(\varphi_k)(\varphi_k)$, as $\mathcal{N} \rightarrow \infty$. Therefore, we obtain

$$\begin{aligned} S_1(\mathcal{N}, M) &\rightarrow_{a.s.} [2\pi]^d \varepsilon(M) \sup_{k \geq 1} \mathcal{R}_{\mathbf{0}, \theta_0}(\varphi_k)(\varphi_k), \quad \mathcal{N} \rightarrow \infty \\ \text{and } \varepsilon(M) \sup_{k \geq 1} \mathcal{R}_{\mathbf{0}, \theta_0}(\varphi_k)(\varphi_k) &\rightarrow 0, \quad M \rightarrow \infty \\ S_2(\mathcal{N}, M) &\rightarrow_{a.s.} 0 \quad \mathcal{N} \rightarrow \infty \\ S_3(M) = \varepsilon(M) \sup_{k \geq 1} \mathcal{R}_{\mathbf{0}, \theta_0}(\varphi_k)(\varphi_k) &\rightarrow 0, \quad M \rightarrow \infty. \end{aligned} \quad (29)$$

Hence, from (28)–(29), we obtain, for $\theta \in \Theta$,

$$\begin{aligned} \sigma_{\mathcal{N}}(\theta) &\rightarrow_{a.s.} \sup_{k \geq 1} \frac{1}{(2\pi)^d} \int_{[-\pi, \pi]^d} \mathcal{F}_{\xi, \theta_0} \mathcal{F}_{\xi, \theta}^{-1}(\varphi_k)(\varphi_k) d\xi \\ &= \sup_{k \geq 1} \frac{1}{(2\pi)^d} \int_{[-\pi, \pi]^d} \mathcal{F}_{\xi, \theta}^{-1} \mathcal{F}_{\xi, \theta_0}(\varphi_k)(\varphi_k) d\xi, \quad \mathcal{N} \rightarrow \infty. \end{aligned} \quad (30)$$

Under (C3),

$$\sup_{k \geq 1} \frac{1}{(2\pi)^d} \int_{[-\pi, \pi]^d} \mathcal{F}_{\xi, \theta_0} \mathcal{F}_{\xi, \theta}^{-1}(\varphi_k)(\varphi_k) d\xi > 1, \quad \theta \neq \theta_0, \quad (31)$$

since, for each $k \geq 1$, $\mathcal{F}_{\xi, \theta_0} \mathcal{F}_{\xi, \theta}^{-1}(\varphi_k)(\varphi_k)$ defines the spectrum of a spatial stationary linear process with unit one-step prediction variance (see Remarks 6–7). Specifically, the variance of such a process is given by $\int_{[-\pi, \pi]^d} \mathcal{F}_{\xi, \theta_0} \mathcal{F}_{\xi, \theta}^{-1}(\varphi_k)(\varphi_k) d\xi$, which must be larger than the one-step prediction variance, unless the spectrum is constant for every $k \geq 1$. This fact does not hold because it means that the composition $\mathcal{F}_{\xi, \theta_0} \mathcal{F}_{\xi, \theta}^{-1}$ of operators $\mathcal{F}_{\xi, \theta_0}$ and $\mathcal{F}_{\xi, \theta}^{-1}$ coincides with the identity operator on $\mathcal{H} + i\mathcal{H}$, which is not possible in view of identifiability condition (C1), since $\theta \neq \theta_0$ in (31). Thus,

$$\inf_{\theta \in \Theta} \sup_{k \geq 1} \frac{1}{(2\pi)^d} \int_{[-\pi, \pi]^d} \mathcal{F}_{\xi, \theta_0} \mathcal{F}_{\xi, \theta}^{-1}(\varphi_k)(\varphi_k) d\xi = 1. \quad (32)$$

From (32), the theoretical counterpart of the empirical loss function (20) attaches the minimum at $\theta = \theta_0$. The strong consistency of the derived parameter estimator follows from this fact, and from equations (30) and (31) (see Appendix for more details).

4 Simulation study

This section illustrates the derived strong consistency of the parameter estimator (19)–(20), as well as its mean-square consistency. We restrict our attention to

the case where the log–intensity random field is a $\text{SAR}\mathcal{H}(1)$ process (see [30]). As commented in the Introduction, in the numerical examples below we address the problem of estimating the hyperparameters, characterizing the point spectra and eigenvectors of the spatial correlation operators, that are also involved in the parameterization of our spectral density operator family (see equation (37) below).

Let, as before, $\mathcal{H} = L^2(\mathcal{T})$ be the space of square–integrable functions on the interval $\mathcal{T} \subseteq \mathbb{R}_+$. Consider the case $d = 2$, and assume that the \mathcal{H} –valued log–intensity random field $\{\varkappa_{\mathbf{z}}, \mathbf{z} \in \mathbb{Z}^2\}$ satisfies the $\text{SAR}\mathcal{H}(1)$ state equation

$$\varkappa_{i,j} = L_1(\varkappa_{i-1,j}) + L_2(\varkappa_{i,j-1}) + L_3(\varkappa_{i-1,j-1}) + \epsilon_{i,j}, \quad (i,j) \in \mathbb{Z}^2, \quad (33)$$

where $\epsilon = \{\epsilon_{i,j}, (i,j) \in \mathbb{Z}^2\}$ denotes a spatial \mathcal{H} –valued zero–mean generalized white noise. Hence, for any spatial node (i,j) , $E|\epsilon_{i,j}(\varphi_k)|^2 = \|\varphi_k\|^2 = \sigma_k^2 = 1$, for $k \geq 1$, with $\{\varphi_k, k \geq 1\}$ being an orthonormal basis of \mathcal{H} . Thus, $\mathcal{R}_{i,j}^\epsilon = E(\epsilon_{i+k,j+l} \otimes \epsilon_{k,l}) = E(\epsilon_{i,j} \otimes \epsilon_{0,0}) = I_{\mathcal{H}}$, for every $(i,j), (k,l) \in \mathbb{Z}^2$, with $I_{\mathcal{H}}$ denoting the identity operator on \mathcal{H} . We work under the assumption of $\{\epsilon_{i,j}, (i,j) \in \mathbb{Z}^2\}$ being Gaussian. Specifically, $\{\epsilon_{i,j}(\varphi_k), k \geq 1, (i,j) \in \mathbb{Z}^2\}$ is a family of independent standard Gaussian random variables. For every $(i,j) \in \mathbb{Z}^2$, $\epsilon_{i,j}$ is uncorrelated with $\varkappa_{i-1,j}$, $\varkappa_{i,j-1}$, $\varkappa_{i-1,j-1}$. The pure point spectra of L_i , $i = 1, 2, 3$, are defined from the pure point spectra of the linear operators involved in the spatial functional infinite–order moving average ($\text{SMA}\mathcal{H}(\infty)$) representation of $\varkappa_{i,j}$.

In the subsequent examples, L_i , $i = 1, 2, 3$, will be introduced in terms of the eigenvectors $\{\phi_k, k \geq 1\}$ of the Dirichlet negative Laplacian operator $(-\Delta)_{\mathcal{T}}$ on an interval \mathcal{T}

$$\phi_k(t) = \sin\left(\frac{\pi tk}{T}\right), \quad t \in \mathcal{T} = [0, T], \quad k \geq 1. \quad (34)$$

Applying Spectral Theorem on Spectral Calculus for self–adjoint operators on a separable Hilbert space (see, e.g., [7], pp. 112–126), we can characterize the pure point spectrum of any continuous function of $(-\Delta)_{\mathcal{T}}$, by applying this function to the eigenvalues of $(-\Delta)_{\mathcal{T}}$. This is the framework adopted in Examples 1 and 2 below for the introduction of operators L_i , $i = 1, 2, 3$. On the other hand, in the case of considering that the functional values of the \mathcal{H} –valued log–intensity process are supported on the entire real line, these models can be extended by considering the weak–sense Fourier transform of Riesz and Bessel potentials (see, e.g., [36]).

Example 1. In this example, we address the problem of estimating parameter $\theta \in \Theta$ characterizing the support $\mathcal{T}(\theta) = [0, \theta]$ of the eigenvectors (34). We thus have $L_{i,\theta}$, $i = 1, 2, 3$, given by

$$\begin{aligned}
L_{1,\theta} &= \Phi_{M_1(\theta)} \mathcal{K}_1(\theta, \pi) (-\Delta)_{\mathcal{T}(\theta)}^{-\beta_1}, \quad L_{2,\theta} = \Phi_{M_2(\theta)} \mathcal{K}_2(\theta, \pi) (-\Delta)_{\mathcal{T}(\theta)}^{-\beta_2}, \\
L_{3,\theta} &= -L_{1,\theta} L_{2,\theta} = -L_{2,\theta} L_{1,\theta},
\end{aligned} \tag{35}$$

where $\Phi_{M_i(\theta)}$ denotes the projection operator onto the subspace generated by the eigenvectors $\phi_1, \dots, \phi_{M_i(\theta)}$ of $(-\Delta)_{\mathcal{T}(\theta)}$, with $M_i(\theta) \geq 1$ being a bounded function in $\theta \in \Theta$, for $i = 1, 2$. Here, $\beta_i, \mathcal{K}_i \in \mathbb{R}_+$ are known, and \mathcal{K}_i is continuous in $\theta \in \Theta$, for $i = 1, 2$. Applying Spectral Theorem on Spectral Calculus for self-adjoint operators on a separable Hilbert space (see, e.g., [7]), the eigenvalues $\{\lambda_{k,i}(\theta), k \geq 1\}$ of the autocorrelation operator $L_{i,\theta}$ are given, for $i = 1, 2, 3$, by

$$\begin{aligned}
\lambda_{k,1}(\theta) &= 1_{[1, M_1(\theta)]}(k) \mathcal{K}_1(\theta, \pi) [\lambda_k((-\Delta)_{\mathcal{T}(\theta)})]^{-\beta_1} \\
\lambda_{k,2}(\theta) &= 1_{[1, M_2(\theta)]}(k) \mathcal{K}_2(\theta, \pi) [\lambda_k((-\Delta)_{\mathcal{T}(\theta)})]^{-\beta_2} \\
\lambda_{k,3}(\theta) &= -\lambda_{k,1}(\theta) \lambda_{k,2}(\theta), \quad k \geq 1, \quad \theta \in \Theta,
\end{aligned} \tag{36}$$

where $1_{[1, M_i(\theta)]}(k)$ denotes the indicator function of the set $[1, M_i(\theta)] \subset \mathbb{N}$, with, as before, $M_i(\theta) \geq 1$, for $i = 1, 2$. For $k \geq 1$, $\lambda_k((-\Delta)_{\mathcal{T}(\theta)})$ denotes the k -th eigenevalue of $(-\Delta)_{\mathcal{T}(\theta)}$. Consider the particular case $M_1(\theta) = M_2(\theta) = M(\theta)$, and assume that $\lambda_{k,i}(\theta)$, $k \geq 1$, $i = 1, 2, 3$, are such that the roots of the polynomial $P_{k,\theta}(z_1, z_2) = \sum_{i=0}^1 \sum_{j=0}^1 p_{k,i,j,\theta} z_1^i z_2^j$, are outside the unit polydisc (i.e., the product of two open unit disks in the complex plane). Here, $p_{k,0,0,\theta} = 1$, $p_{k,1,0,\theta} = \lambda_{k,1}(\theta)$, $p_{k,0,1,\theta} = \lambda_{k,2}(\theta)$, and $p_{k,1,1,\theta} = -\lambda_{k,1}(\theta) \lambda_{k,2}(\theta)$, $k \geq 1$. From equations (33)–(36), we compute the spectral density operator, given by, for $\xi \in [-\pi, \pi]^2$,

$$\begin{aligned}
&\mathcal{F}_{\xi,\theta}(\phi_{k,\theta})(\phi_{k,\theta}) = \\
&= \frac{1}{|1 - \lambda_{k,1}(\theta) \exp(i\xi_1) - \lambda_{k,2}(\theta) \exp(i\xi_2) - \lambda_{k,3}(\theta) \exp(i(\xi_1 + \xi_2))|^2} \tag{37} \\
&L_{q,\theta}(g)(h) = \sum_{k=1}^{\infty} \lambda_{k,q}(\theta) \langle \phi_{k,\theta}, h \rangle \langle \phi_{k,\theta}, g \rangle, \quad \forall g, h \in \mathcal{H}, \quad q = 1, 2, 3 \\
&\phi_{k,\theta}(t) = \sin\left(\frac{\pi t k}{\theta}\right), \quad t \in \mathcal{T}(\theta) = [0, \theta], \quad k \in [1, M(\theta)], \quad \theta \in \Theta.
\end{aligned}$$

Under the conditions assumed on model parameters (36), **Assumption A2** is satisfied in our SARH(1) framework, as follows from Corollary 2.3 in [2], applying similar results to those obtained in Corollary 4.1 and Theorem 4.8 of this monograph. Parameter θ univocally defines the support $\mathcal{T}(\theta)$ of the eigenvectors of the Dirichlet negative Laplacian operator. Hence, the identifiability condition (C1) is satisfied. Conditions (15), (C2) and (C4) are obtained from

Table 1: Location parameter estimates. Sample Mean, Standard Deviation, and Empirical Mean Square Errors (M.S.E.), from 100 generations, $\theta_0 = 1$

\mathcal{N}	$\widehat{\theta}_{\mathcal{N}}$	$\sigma(\widehat{\theta}_{\mathcal{N}})$	M.S.E
40000	0.9867	0.1391	0.0193
62500	1.0066	0.0972	0.0094
90000	0.9993	0.0857	0.0073
122500	1.0008	0.0810	0.0065
160000	1.0034	0.0716	0.0051
202500	0.9893	0.0536	0.0030
250000	0.9995	0.0449	0.0020
302500	1.0060	0.0436	0.0019

equations (36)–(37), under the restrictions considered on the parametric coefficients $\{\lambda_{k,i}(\theta), k \in [1, M(\theta)], \theta \in \Theta, i = 1, 2\}$, defining the polynomial family $\{P_{k,\theta}, k \in [1, M(\theta)], \theta \in \Theta\}$. Condition (C3) also holds since $\sigma_k^2 = 1$, for every $k \geq 1$. The strong-consistency of the SAR $\mathcal{H}(1)$ plug-in parametric predictor

$$\widehat{\mathcal{X}}_{i,j}^{\mathcal{N}}(\theta) = L_{1,\widehat{\theta}_{\mathcal{N}}} \mathcal{X}_{i-1,j} + L_{2,\widehat{\theta}_{\mathcal{N}}} \mathcal{X}_{i,j-1} + L_{3,\widehat{\theta}_{\mathcal{N}}} \mathcal{X}_{i-1,j-1}, \quad \forall (i,j) \in \mathbb{Z}^2, \quad (38)$$

is then obtained under similar conditions to those assumed in [2] in the AR $\mathcal{H}(1)$ framework. The estimation results are displayed in Table 1 and Figure 1, where we have considered $\theta_0 = 1$, $\mathcal{K}_1(\theta, \pi) = \frac{\theta^{2-11/10}}{\pi^{2-11/10}}$, $\mathcal{K}_2(\theta, \pi) = \frac{\theta^{2-12/10}}{\pi^{2-12/10}}$, $\beta_1 = \frac{11}{20}$, $\beta_2 = \frac{12}{20}$, $M(\theta) = [10\theta]$, and $\theta \in \Theta = [0.7, 4]$, with $[\cdot]$ denoting the integer part function. We have tested the spatial functional sample sizes $\mathcal{N} = 40000, 62500, 90000, 122500, 160000, 202500, 250000, 302500$. Specifically, Figure 1–left displays the sample values of $\widehat{\theta}_{\mathcal{N}}$, based on 100 generations of each functional sample. The empirical mean quadratic errors are also computed in Table 1 and Figure 1–right.

Example 2. Let now consider the following parametric family of autocorrelation

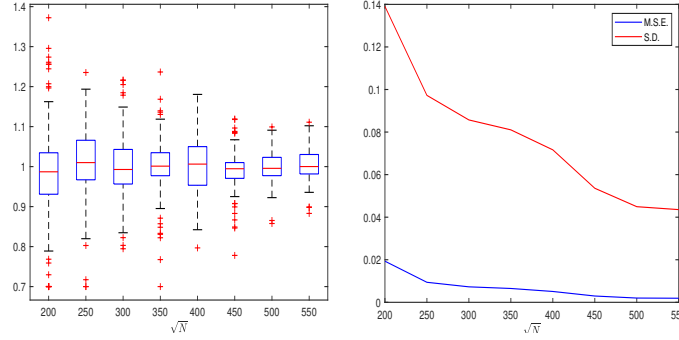


Figure 1: Boxplots of the sample values of $\hat{\theta}_N$, for $\theta_0 = 1$ (left-plot). Empirical Mean Square Errors (M.S.E), blue line, and Standard Deviations (S.D.), red line.

operators L_{q,θ_q} , $q = 1, 2$,

$$\begin{aligned}
L_{1,\theta_1} &= \Phi_M \theta_{1,1} \left[\theta_{1,2} + (1/\pi)(-\Delta)_{[0,1]}^{1/2} \right]^{-1} \\
L_{2,\theta_2} &= \Phi_M \theta_{2,1} \left[\theta_{2,2} + (1/\pi)(-\Delta)_{[0,1]}^{1/2} \right]^{-1}, \quad (\theta_1, \theta_2) \in \Theta \\
L_{3,\theta_3} &= -L_{1,\theta_1} L_{2,\theta_2} = -L_{2,\theta_2} L_{1,\theta_1} \\
\phi_k(t) &= \sin(\pi t k), \quad t \in [0, 1], \quad k \geq 1 \\
\lambda_{k,q}(\theta_q) &= 1_{[1,M]}(k) \frac{\theta_{q,1}}{k + \theta_{q,2}}, \quad q = 1, 2, \quad \lambda_{k,3}(\theta_3) = -\lambda_{k,1}(\theta_1) \lambda_{k,2}(\theta_2), \quad k \geq 1
\end{aligned} \tag{39}$$

where, as before, $1_{[1,M]}(k)$ is the indicator function of the set $[1, M] \subset \mathbb{N}$, Φ_M , $M \geq 1$, denotes the projection operator onto the subspace generated by the eigenvectors ϕ_1, \dots, ϕ_M of Dirichlet negative Laplacian operator $(-\Delta)_{[0,1]}$ on the interval $[0, 1]$. Here, $\{\lambda_{k,1}(\theta_1), \lambda_{k,2}(\theta_2), k \geq 1, (\theta_1, \theta_2) \in \Theta\}$ is the parametric family of eigenvalues of the autocorrelation operators $\{L_{1,\theta_1}, L_{2,\theta_2}, (\theta_1, \theta_2) \in \Theta\}$. Under similar conditions to Example 1 on these parametric families of eigenvalues of $\{L_{1,\theta_1}, L_{2,\theta_2}, (\theta_1, \theta_2) \in \Theta\}$, Assumptions A1–A2, and conditions (15) and (C1)–(C4) hold. Thus, the strong-consistency of the parameter estimator $\hat{\theta}_N$ follows from Theorem 1. Particularly, we have considered the scale parameter values $\theta_{1,1} = 1$, $\theta_{2,1} = 1.5$, and the location parameters values $\theta_{1,2} = 1.6$, and $\theta_{2,2} = 1.2$, lying in the interior of $\Theta = ([0.7, 1.3] \times [1.3, 1.9]) \times ([1.2, 1.8] \times [0.9, 1.5])$. See the numerical results displayed at the left-plots of Figures 2–5, from 100 generations of each one of the spatial functional samples of sizes $N = 40000, 62500, 90000, 122500, 160000$,

202500, 250000, 302500. The empirical mean quadratic errors have also been computed for these sample sizes (see right-plots of Figures 2–5 and Table 2). It can also be observed a good performance of the proposed estimation methodology, for the considered spatial functional samples sizes, and the chosen truncation parameter value $M = 10$. Note that this truncation parameter value provides the threshold dimension to ensure a stable behavior of the parameter vector estimator, with respect to the input spatial functional data, according to the temporal discretization step size and smoothing considered.

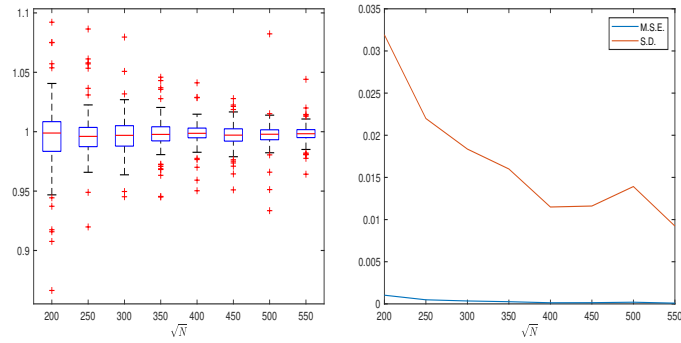


Figure 2: Boxplots of the sample values of $\hat{\theta}_{1,1,N}$, for $\theta_{1,0} = 1$, based on 100 generations (left-plot). Empirical Mean Square Errors (M.S.E.), blue line, and Sample Standard Deviation (S.D.), red line (right-plot)

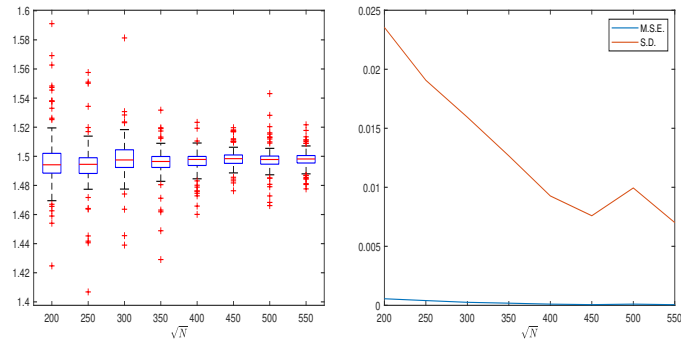


Figure 3: Boxplots of the sample values of $\hat{\theta}_{2,1,N}$, for $\theta_{2,0} = 1.5$, based on 100 generations (left-plot). Empirical Mean Square Errors (M.S.E.), blue line, and Sample Standard Deviation (S.D.), red line (right-plot)

Table 2: Location and scale parameter estimates. Sample Mean, Standard Deviation and Empirical Mean Quadratic Errors (M.S.E.), from 100 generations, $\theta_{1,1,0} = 1$, $\theta_{2,1,0} = 1.5$, $\theta_{1,2,0} = 1.6$, and $\theta_{2,2,0} = 1.2$.

\mathcal{N}	$\overline{\hat{\theta}_{1,1,\mathcal{N}}}$	$\sigma(\hat{\theta}_{1,1,\mathcal{N}})$	M.S.E.
40000	0.9955	0.0319	0.00103
62500	0.9975	0.0220	0.00048
90000	0.9965	0.0184	0.00035
122500	0.9978	0.0160	0.00026
160000	0.9984	0.0115	0.00013
202500	0.9969	0.0116	0.00014
250000	0.9973	0.0139	0.00020
302500	0.9983	0.0092	0.00009

\mathcal{N}	$\overline{\hat{\theta}_{2,1,\mathcal{N}}}$	$\sigma(\hat{\theta}_{2,1,\mathcal{N}})$	M.S.E.
40000	1.4972	0.0236	0.00056
62500	1.4934	0.0191	0.00040
90000	1.4980	0.0159	0.00026
122500	1.4951	0.0127	0.00018
160000	1.4959	0.0093	0.00010
202500	1.4989	0.0076	0.00006
250000	1.4977	0.0099	0.00010
302500	1.4979	0.0070	0.00005

\mathcal{N}	$\overline{\hat{\theta}_{1,2,\mathcal{N}}}$	$\sigma(\hat{\theta}_{1,2,\mathcal{N}})$	M.S.E.
40000	1.6003	0.0205	0.00042
62500	1.5991	0.0148	0.00022
90000	1.6018	0.0109	0.00012
122500	1.5998	0.0159	0.00025
160000	1.6001	0.0058	0.00003
202500	1.6008	0.0019	0.00000
250000	1.6011	0.0075	0.00006
302500	1.6005	0.0040	0.00002

\mathcal{N}	$\overline{\hat{\theta}_{2,2,\mathcal{N}}}$	$\sigma(\hat{\theta}_{2,2,\mathcal{N}})$	M.S.E.
40000	1.2046	0.0268	0.00073
62500	1.2054	0.0151	0.00026
90000	1.2024	0.0321	0.00103
122500	1.2027	0.0083	0.00007
160000	1.2015	0.0067	0.00005
202500	1.2005	0.0030	0.00001
250000	1.2008	0.0065	0.00004
302500	1.2008	0.0023	0.00001

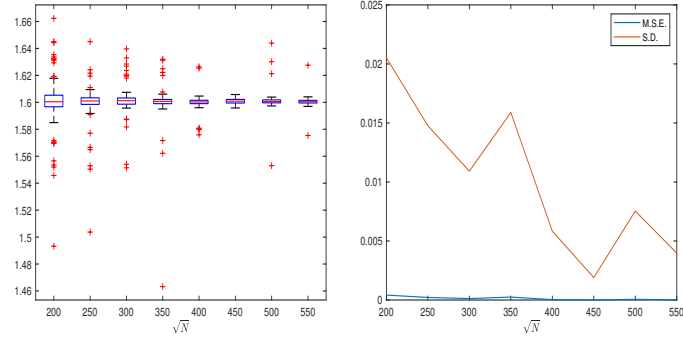


Figure 4: Boxplots of sample values of $\hat{\theta}_{1,2,N}$, for $\theta_{1,2,0} = 1.6$, based on 100 generations (left-plot). Empirical Mean Square Errors (M.S.E.), blue line, and Sample Standard Deviation (S.D.), red line (right-plot)

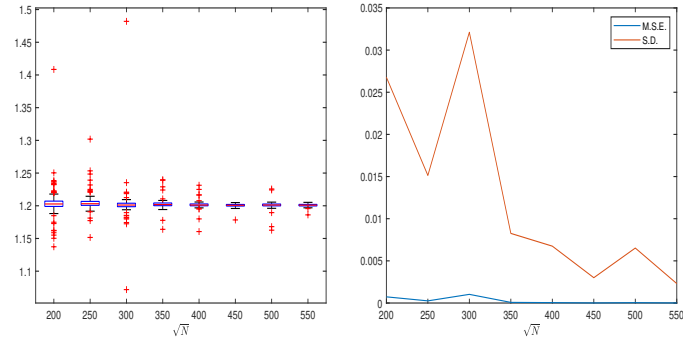


Figure 5: Boxplots of sample values of $\hat{\theta}_{2,2,N}$, for $\theta_{2,2,0} = 1.2$, based on 100 generations (left-plot). Empirical Mean Square Errors (M.S.E.), blue line, and Sample Standard Deviation (S.D.), red line (right-plot)

5 Real-data example

Data are reported by the Spanish National Statistical Institute, consisting of 432 monthly records on the number of respiratory disease mortality cases at the 48 Spanish provinces in the Iberian Peninsula, during the period 1980–2015. A spatial heterogeneous 10th-degree polynomial trend model fitting is achieved after suitable preprocessing of our original data set. Spatial functional residual correlation analysis is performed in the spectral domain, in terms of the $\text{SAR}\mathcal{H}(1)$ model introduced in the previous section. Specifically, the main steps of the implemented estimation algorithm are the following.

- Step 1. The cumulative number of mortality cases at the 48 Spanish provinces, in the period 1980–2015, are computed from the 432 monthly records.
- Step 2. The step cumulative mortality curves in Step 1 are interpolated at 1725 temporal nodes, and cubic B-spline smoothed.
- Step 3. The curve data in Step 2 are spatially interpolated to a $\mathcal{N} = 20 \times 20$ regular grid, by applying Inverse Distance Weighting interpolation.
- Step 4. The derivatives and logarithm transforms of the curve data in Step 3 provide the functional values of the log–intensity at the spatial nodes of the $\mathcal{N} = 20 \times 20$ regular grid.
- Step 5. Least-squares polynomial fitting is implemented to approximate the log–intensity curve trend at each spatial node.
- Step 6. The residual log–intensity curve values obtained in Step 5 are projected onto the orthonormal basis $\{\sin(\pi pt/1725), p \geq 1\}$ of $L^2([0, 1725])$.
- Step 7. The projections in Step 6 are spatially normalized.
- Step 8. The two–dimensional Fast Fourier Transform is applied to the outputs of Step 7.
- Step 9. The empirical loss function $\sigma_{400}(\boldsymbol{\theta})$ in (20) is computed from Step 8.
- Step 10. Model (37) is fitted by computing the minimum of the constrained nonlinear multivariate function $\sigma_{400}(\boldsymbol{\theta})$. Here, L_3 is not necessarily given by the composition of operators $L_i, i = 1, 2$, as in the previous section. We have used the option 'lbfgs' of *fmincon* MatLab function, which is an optimization algorithm in the family of quasi-Newton methods, involving an inverse Hessian matrix estimate to steer its search through variable space.

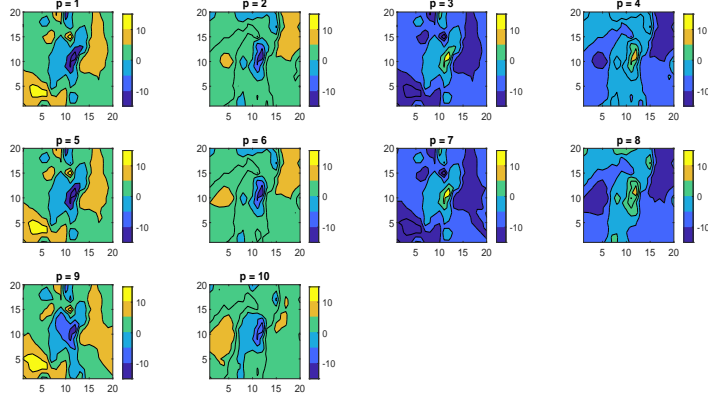


Figure 6: Ten normalized projections of the spatial functional residual log-intensity

Step 11. The $\text{SARH}(1)$ plug-in parametric predictor (38) is obtained from Step 10.

Our parametric model fitting has been performed in terms of the spectral kernel defined by the eigenvectors $\{\sin(\pi p t / 1725), p \geq 1\}$ of the Dirichlet negative Laplacian operator on $L^2([0, 1725])$. The least-squares estimate of Cox process values are obtained from Step 11 applying (5) in terms of $\{\sin(\pi p t / 1725), p \geq 1\}$, and the corresponding inverse projection formula. Figures 6–7 respectively show the original and estimated spatial projections of the functional residual log-intensity random field, for the truncation parameter $M = 10$ (see outputs from Steps 6–7 and 10).

In Steps 9–10, we have fitted the following parametric model

$$\hat{\lambda}_{p,i} = \lambda_{p,i}(\hat{\boldsymbol{\theta}}_{i,\mathcal{N}}) = \hat{\theta}_{i,1,\mathcal{N}} + |\sin(p\pi/2)| \hat{\theta}_{i,2,\mathcal{N}}(p), \quad p = 1, \dots, 10, \quad i = 1, 2, 3, \quad (40)$$

for the eigenvalues of $L_{i,\hat{\boldsymbol{\theta}}_{i,\mathcal{N}}}$, $i = 1, 2, 3$, considering $M = 10$, from a functional sample size $\mathcal{N} = 400$. The fitted parameter values $\hat{\boldsymbol{\theta}}_{i,\mathcal{N}}$, $i = 1, 2, 3$, are the

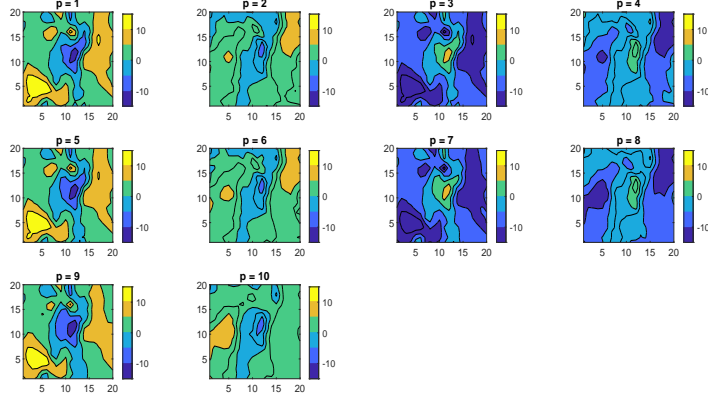


Figure 7: Estimates of the normalized projections of the spatial functional residual log-intensity

following:

$$\begin{aligned}
&\hat{\theta}_{1,1,\mathcal{N}} = 0.56; \quad \hat{\theta}_{1,2,\mathcal{N}}(p) = 0, \quad p = 2, 4, 6, 8, 10; \\
&\hat{\theta}_{1,2,\mathcal{N}}(p) = 0.08, \quad p = 1, 3, 5; \quad \hat{\theta}_{1,2,\mathcal{N}}(p) = 0.189; \quad p = 7, 9; \\
&\hat{\theta}_{2,1,\mathcal{N}} = 0.28; \quad \hat{\theta}_{2,2,\mathcal{N}}(p) = 0, \quad p = 1, 2, 3, 4, 5, 6, 8, 10; \\
&\hat{\theta}_{2,2,\mathcal{N}}(7) = 0.0725; \quad \hat{\theta}_{2,2,\mathcal{N}}(9) = 0.0814; \quad \hat{\theta}_{3,1,\mathcal{N}} = 0.0033; \\
&\hat{\theta}_{3,2,\mathcal{N}}(p) = -0.0052, \quad p = 2, 4, 6; \quad \hat{\theta}_{3,2,\mathcal{N}}(p) = 0, \quad p = 8, 10; \\
&\hat{\theta}_{3,2,\mathcal{N}}(p) = 0.4444, \quad p = 1, 3, 5; \quad \hat{\theta}_{3,2,\mathcal{N}}(p) = 0, \quad p = 7, 9, \quad \mathcal{N} = 400.
\end{aligned} \tag{41}$$

The corresponding parametric estimations $\left\{ \lambda_{p,i}(\hat{\theta}_{i,\mathcal{N}}), \quad p = 1, \dots, 10 \right\}$, $i = 1, 2, 3$, of the point spectra of $L_{i,\hat{\theta}_{i,\mathcal{N}}}$, $i = 1, 2, 3$, are displayed in Table 3 and Figure 8. Finally, the original respiratory–disease–mortality log-intensity curves (dashed blue line), and their estimations (red line), at the 48 Spanish provinces, are displayed in Figures 9–10. The worst (Soria province) and the best (Pontevedra province) model fitting are zoomed in Figure 11. Also, the original and estimated annually averaged respiratory–disease–mortality risk maps are displayed in Figure 12.

To assess spatial functional prediction ability of our approach, cross-validation is implemented. By leaving aside the curves observed at the nodes in a neighborhood of the province defining the region of interest (the validation functional data set), Steps 1–11 are run in terms of the remaining func-

	$\lambda_{p,1}(\widehat{\boldsymbol{\theta}}_{1,\mathcal{N}})$	$\lambda_{p,2}(\widehat{\boldsymbol{\theta}}_{2,\mathcal{N}})$	$\lambda_{p,3}(\widehat{\boldsymbol{\theta}}_{3,\mathcal{N}})$
$p = 1$	0.6578	0.2801	0.4493
$p = 2$	0.5534	0.2878	-0.0102
$p = 3$	0.6583	0.2812	0.4482
$p = 4$	0.5547	0.2873	-0.0091
$p = 5$	0.6595	0.2841	0.4456
$p = 6$	0.5572	0.2860	-0.0061
$p = 7$	0.7490	0.3525	0.1316
$p = 8$	0.5620	0.2819	0.0021
$p = 9$	0.7507	0.3614	0.1211
$p = 10$	0.5678	0.2634	0.0398

Table 3: Point spectra estimates of $L_{i,\widehat{\boldsymbol{\theta}}_{i,\mathcal{N}}}$, $i = 1, 2, 3$, for $M = 10$, $\mathcal{N} = 400$

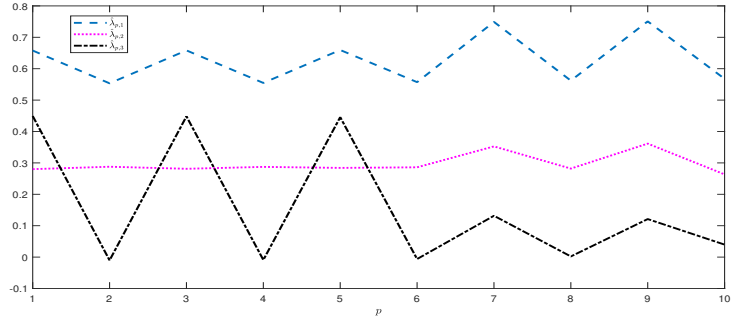


Figure 8: Plot of point spectra estimates of $L_{i,\widehat{\boldsymbol{\theta}}_{i,\mathcal{N}}}$, $i = 1, 2, 3$, for $M = 10$ and $\mathcal{N} = 400$. In the plot, we have used the notation $\widehat{\lambda}_{p,i} = \lambda_{p,i}(\widehat{\boldsymbol{\theta}}_{i,\mathcal{N}})$, for $p = 1, \dots, 10$, $i = 1, 2, 3$

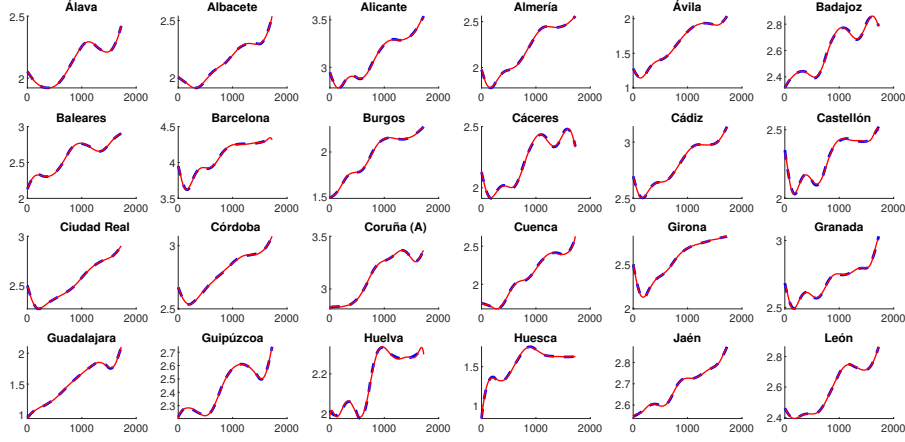


Figure 9: Original respiratory–disease–mortality log–intensity curves (dashed blue line), and their respective estimates (red line), for the above 24 Spanish provinces displayed

tional observations, spatially distributed at the neighborhoods of the rest of the Spanish provinces (the training functional data set). The corresponding $\text{SARH}(1)$ plug-in parametric predictor (38) is computed at each iteration. After 48 iterations, the mean cross-validation functional absolute relative error $\text{CVFARE}(t) = \frac{1}{48} \sum_{\mathbf{z} \in \mathcal{R}} \left| \frac{\kappa_{\mathbf{z}}(t) - \hat{\kappa}_{\mathbf{z}}(t)}{\kappa_{\mathbf{z}}(t)} \right|$, $t = 1, \dots, 1725$, is obtained, where \mathcal{R} denotes the set of latitudes and longitudes defining the spatial locations of the 48 Spanish provinces. Table 4 displays the annual mean of the pointwise values of CVFARE. The empirical value $\|\text{CVFARE}\|_{L^1([0,1725])} = 0.0016$ computed from Table 4 shows a good spatial functional predictive ability of the presented approach beyond the log–Gaussian scenario.

6 Concluding remarks

The results derived in this paper can be easily reformulated for \mathcal{H} –valued spatially continuous log–intensity models, replacing the index set $[-\pi, \pi]^d$ by \mathbb{R}^d , and adapting the subsequent conditions to an unbounded frequency domain, in the definition of our spectral density operator family. Indeed, one can adopt our discrete spatial parametric framework for practical purposes, considering constant functional values over the spatial regular grid quadrants ([29]). As usual, for the approximation of a continuous log–intensity model, interpolation and smoothing techniques can be implemented. For example, spatial smoothing based on spline bases has been widely applied during the last decades, since the eighties (see,

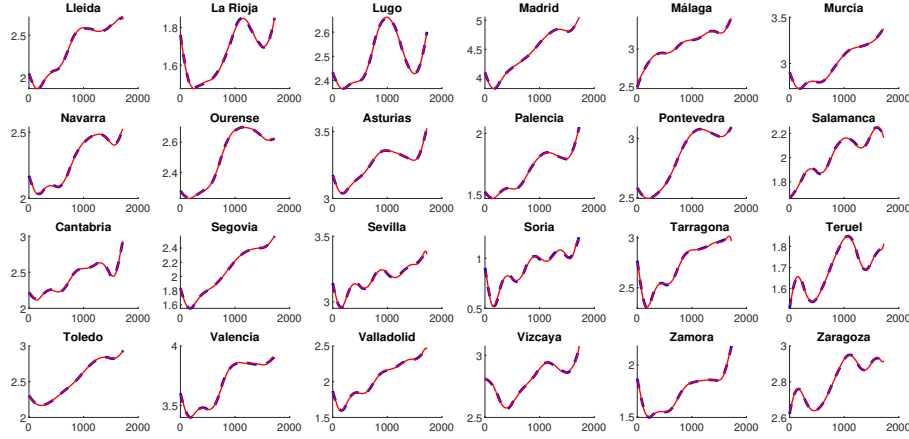


Figure 10: Original respiratory–disease–mortality log–intensity curves (dashed blue line), and their respective estimates (red line), for the above 24 Spanish provinces displayed

e.g., [27]).

Several problems remain open in the field of FDA techniques applied to the statistical analysis of spatial point patterns (see, e.g., [18]; [31]; [11]; [5], among others). This paper provides a spatial functional spectral–based approach, in the parametric estimation of the second order moments of the Cox process family, driven by a spatial \mathcal{H} –valued log–intensity. The corresponding functional analysis of variance can also be achieved from the derived parametric predictor. One of the key problems to be faced, in a near future, is the definition of a multivariate version of the introduced point process class, as well as its spectral functional estimation in an infinite–dimensional multivariate framework. This subject constitutes the topic of a subsequent paper.

Appendix. Proof of Theorem 1

In the derivation of the proof of Theorem 1, the truncated empirical expansion of the periodogram operator

$$\begin{aligned}
\mathcal{I}_{\xi}^{\mathcal{N}}(\varphi_k)(\varphi_l) &= \tilde{X}_{\xi}^{\mathcal{N}}(\varphi_k) \tilde{X}_{-\xi}^{\mathcal{N}}(\varphi_l) \\
&= \frac{1}{(2\pi)^d} \sum_{\mathbf{z} \in \prod_{i=1}^d [-\mathcal{N}_i+1, \mathcal{N}_i-1]} \mathcal{C}(\mathbf{z}, k, l) \exp \left(-i \sum_{j=1}^d \xi_j z_j \right), \quad k, l \geq 1 \\
&\quad \mathbf{z} = (z_1, \dots, z_d) \in \mathbb{Z}^d, \quad z_i \in [-\mathcal{N}_i+1, \mathcal{N}_i-1], \quad i = 1, \dots, d \quad (42)
\end{aligned}$$

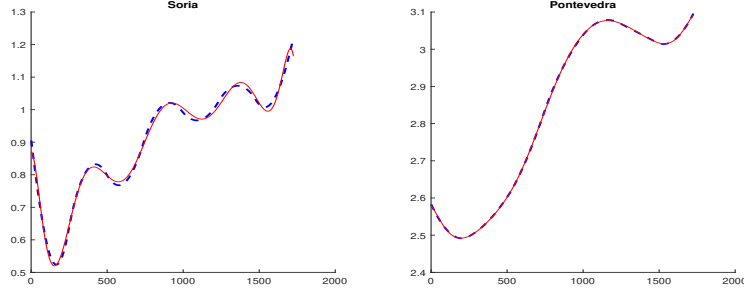


Figure 11: Spanish provinces with largest, Soria (left), and smallest, Pontevedra (right), $L^1([0, 1725])$ -norm of the associated functional absolute relative error are shown. Original curves are plotted in dashed blue line, and estimated curves are represented in red line.

Table 4: ACVFARE. Pointwise annually averaged CVFARE obtained from the validations

Year	ACVFARE	Year	ACVFARE	Year	ACVFARE	Year	ACVFARE
1980	0.00301	1989	0.00322	1998	0.00135	2007	0.00007
1981	0.00273	1990	0.00245	1999	0.00036	2008	0.00008
1982	0.00137	1991	0.00073	2000	0.00106	2009	0.00008
1983	0.00295	1992	0.00116	2001	0.00191	2010	0.00053
1984	0.00139	1993	0.00315	2002	0.00134	2011	0.00124
1985	0.00192	1994	0.00357	2003	0.00033	2012	0.00092
1986	0.00323	1995	0.00129	2004	0.00085	2013	0.00159
1987	0.00175	1996	0.00276	2005	0.00100	2014	0.00142
1988	0.00118	1997	0.00244	2006	0.00045	2015	0.00230

in terms of the Fourier coefficients introduced in (25) is first applied. At the same time, the truncated Fourier series (26) defined from the Fourier coefficients

$$\begin{aligned}
g(\mathbf{z}, \theta, k) &= \frac{1}{(2\pi)^d} \int_{[-\pi, \pi]^d} \exp \left(i \sum_{j=1}^d \varpi_j z_j \right) \mathcal{F}_{\varpi, \theta}^{-1}(\varphi_k)(\varphi_k) d\varpi \\
\mathbf{z} &= (z_1, \dots, z_d) \in \mathbb{Z}^d, \quad \theta \in \Theta, \quad k \geq 1,
\end{aligned} \tag{43}$$

of the inverse $\mathcal{F}_{\varpi, \theta}^{-1}$ of the spectral density operator is also considered. Equations (42)–(43) are applied in the derivation of the convergence to zero of equations (27) and (28). Specifically, let $\xi_{z_j} = \frac{2\pi z_j}{\mathcal{N}_j}$, with $z_j \in \mathbb{Z}$ such that $-\frac{\mathcal{N}_j}{2} < z_j \leq \left\lceil \frac{\mathcal{N}_j}{2} \right\rceil$, for $j = 1, \dots, d$, and $\mathcal{N} = \prod_{j=1}^d \mathcal{N}_j$ being the functional sample size.

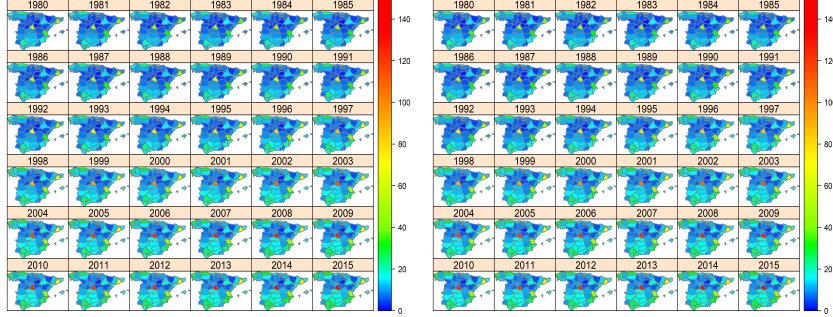


Figure 12: Observed (left) and estimated (right) annually averaged respiratory-disease-mortality risk maps, during the period 1980–2015

Applying Parseval identity in $L^2([-\pi, \pi]^d)$, for M fixed large, and $\theta \in \Theta$,

$$\begin{aligned} & \frac{(2\pi)^d}{\mathcal{N}} \sum_{\mathbf{z}_j} \left| q_{\boldsymbol{\xi}_{\mathbf{z}_j}, \theta}^M \mathcal{I}_{\boldsymbol{\xi}_{\mathbf{z}_j}}^{(\mathcal{N})}(\varphi_k)(\varphi_k) - q_{\boldsymbol{\xi}_{\mathbf{z}_j}, \theta}^M \mathcal{F}_{\boldsymbol{\xi}_{\mathbf{z}_j}, \theta_0}(\varphi_k)(\varphi_k) \right|^2 \\ &= \frac{(2\pi)^d}{\mathcal{N}} \sum_{u_j \in [-M_j+1, M_j-1], j=1, \dots, d} \left| \prod_{j=1}^d \left(1 - \frac{|u_j|}{M_j} \right) g(\mathbf{u}, \theta, k) \right|^2 \\ & \quad \times \left| [\mathcal{C}(\mathbf{u}, k, k) + \mathcal{K}(\mathcal{N})] - \mathcal{R}_{\mathbf{u}, \theta_0}(\varphi_k)(\varphi_k) \right|^2, \quad (44) \end{aligned}$$

where $\mathcal{K}(\mathcal{N}) \rightarrow 0$, as $\mathcal{N} \rightarrow \infty$ (see [17]). **Assumption A2** then implies the a.s. convergence to zero of (44), as $\mathcal{N} \rightarrow \infty$, uniformly in $k \geq 1$, in view of equation (24).

We now proceed to detail the derivation of the strong-consistency of $\hat{\theta}_{\mathcal{N}}$, from equations (30) and (31). Specifically, if, as $\mathcal{N} \rightarrow \infty$, $\hat{\theta}_{\mathcal{N}}$ does not converge a.s. to θ_0 , there exists a subsequent $\hat{\theta}_{\mathcal{N}_m}$ converging to $\theta' \neq \theta_0$, as $m \rightarrow \infty$ ($\mathcal{N}_m \rightarrow \infty$), such that $\theta' \in \Theta$. From (30), for a given positive constant $\eta > 0$, the a.s. lower limit $\underline{\lim}_{\mathcal{N}_m \rightarrow \infty} \sigma_{\mathcal{N}_m}(\hat{\theta}_{\mathcal{N}_m})$ satisfies

$$\underline{\lim}_{\mathcal{N}_m \rightarrow \infty} \sigma_{\mathcal{N}_m}(\hat{\theta}_{\mathcal{N}_m}) \geq \sup_{k \geq 1} \frac{1}{[2\pi]^d} \int_{[-\pi, \pi]^d} \mathcal{F}_{\boldsymbol{\xi}, \theta_0} [\mathcal{F}_{\boldsymbol{\xi}, \theta'} + \eta I_{\mathcal{H} + i\mathcal{H}}]^{-1}(\varphi_k)(\varphi_k) d\boldsymbol{\xi},$$

where $I_{\mathcal{H} + i\mathcal{H}}$ denotes the identity operator on $\mathcal{H} + i\mathcal{H}$. From equation (31), for η sufficiently small, $\underline{\lim}_{\mathcal{N}_m \rightarrow \infty} \sigma_{\mathcal{N}_m}(\hat{\theta}_{\mathcal{N}_m}) > 1$, a.s. On the other hand, for every $\theta \in \Theta$, $\overline{\lim}_{\mathcal{N}_m \rightarrow \infty} \sigma_{\mathcal{N}_m}(\hat{\theta}_{\mathcal{N}_m}) \leq \overline{\lim}_{\mathcal{N}_m \rightarrow \infty} \sigma_{\mathcal{N}_m}(\theta)$, a.s. Hence, for every $\theta \in \Theta$,

$$\overline{\lim}_{\mathcal{N}_m \rightarrow \infty} \sigma_{\mathcal{N}_m}(\hat{\theta}_{\mathcal{N}_m}) \leq \sup_{k \geq 1} \frac{1}{[2\pi]^d} \int_{[-\pi, \pi]^d} \mathcal{F}_{\boldsymbol{\xi}, \theta_0} \mathcal{F}_{\boldsymbol{\xi}, \theta}^{-1}(\varphi_k)(\varphi_k) d\boldsymbol{\xi},$$

which implies the a.s. inequality

$$\overline{\lim}_{\mathcal{N}_m \rightarrow \infty} \sigma_{\mathcal{N}_m}(\hat{\theta}_{\mathcal{N}_m}) \leq \inf_{\theta \in \Theta} \sup_{k \geq 1} \frac{1}{[2\pi]^d} \int_{[-\pi, \pi]^d} \mathcal{F}_{\xi, \theta_0} \mathcal{F}_{\xi, \theta}^{-1}(\varphi_k)(\varphi_k) d\xi = 1,$$

in view of (32), leading to a contradiction. Therefore, $\theta' = \theta_0 = \lim_{\mathcal{N} \rightarrow \infty} \hat{\theta}_{\mathcal{N}}$, a.s., as we wanted to prove.

Acknowledgements

This work has been supported in part by projects PGC2018-099549-B-I00, MTM2016-78917-R, and PID2019-107392RB-I00 of the Ministerio de Ciencia, Innovación y Universidades, Spain (co-funded with FEDER funds), and ERDF Operational Programme 2014–2020 and the Economy and Knowledge Council of the Regional Government of Andalusia, Spain (A-FQM-345-UGR18).

References

- [1] Baddeley A, Gregori P, Mateu J, Stoica R, Stoyan D (2006) Case Studies in Spatial Point Process Modeling. Springer, New York
- [2] Bosq D (2000) Linear Processes in Function Spaces. Lecture Notes in Statistics 149. Springer, New York.
- [3] Bosq D, Ruiz-Medina MD (2014) Bayesian estimation in a high dimensional parameter framework. Electron J Statist 8:1604–1640
- [4] Cox DR (1955) Some statistical methods connected with series of events. J R Statist Soc B 17:129–164
- [5] Dai X, Müller HG (2018) Principal component analysis for functional data on Riemannian manifolds and spheres. Ann Statist 46:3334–3361
- [6] Daley D, Vere-Jones D (2008) An Introduction to the Theory of Point Processes Vol II: General Theory and Structure. Springer-Verlag, New York
- [7] Dautray, R, Lions, JL (1985) Mathematical Analysis and Numerical Methods for Science and Technology Vol 3: Spectral Theory and Applications. Springer, New York.
- [8] Diggle PJ (2013) Statistical Analysis of Spatial and Spatio-Temporal Point Patterns. Taylor & Francis, Boca Raton

- [9] Diggle PJ, Kaimi I, Abellana R (2010) Partial-likelihood analysis of spatio-temporal point-process data. *Biometrics* 66:347–354
- [10] Diggle PJ, Moraga P, Rowlingson B, Taylor BM (2013) Spatial and spatio-temporal log-Gaussian Cox processes: Extending the Geostatistical paradigm. *Stat Sci* 28:542–563
- [11] Goia A , Vieu P (2016) An introduction to recent advances in high/infinite dimensional statistics. *J Multivariate Anal* 146:1–6
- [12] Goncalves FB, Gamerman D (2018) Exact Bayesian inference in spatio-temporal Cox processes driven by multivariate Gaussian processes. *J R Statist Soc B* 80:157–175
- [13] González JA, Rodríguez-Cortés FJ, Cronie O, Mateu J (2016) Spatio-temporal point process statistics: A review. *Spat Stat* 18:505–544
- [14] Grandell J (1976) Doubly Stochastic Process. Springer-Verlag, New York
- [15] Guan Y (2006) A composite likelihood approach in fitting spatial point process models. *J Am Statist Ass* 101:1502–1512
- [16] Guan Y, Waagepetersen R, Beale CM (2008) Second-Order analysis of inhomogeneous spatial point processes with proportional intensity functions. *J Am Statist Ass* 103:769–777
- [17] Hannan EJ (1973) The asymptotic theory of linear time-series models. *J Appl Probab* 10:130–145
- [18] Horváth L, Kokoszka P (2012) Inference for Functional Data with Applications. Springer, New York
- [19] Illian J, Penttinen A, Stoyan H, Stoyan D (2008) Statistical Analysis and Modelling of Spatial Point Patterns. John Wiley & Sons, New York
- [20] Jalilian A, Guan Y, Waagepetersen R (2013) Decomposition of variance for spatial Cox processes. *Scand J Stat* 40:119–137
- [21] Jalilian A, Guan Y, Mateu J, Waagepetersen R (2015) Multivariate product-shot-noise Cox point process models. *Biometrics* 71:1022–1033
- [22] Jalilian A, Guan Y, Waagepetersen R (2019) Orthogonal series estimation of the pair correlation function of a spatial point process. *Stat Sin* 29:769–787

- [23] Ledoux M, Talagrand M (1991). Probability in Banach Spaces: Isoperimetry and Processes. *Ergebnisse der Mathematik und Ihrer Grenzgebiete [Results in Mathematics and Related Areas (3)]* 23. Springer, Berlin.
- [24] Møller J, Syversveen AR, Waagepetersen R (1998) Log Gaussian Cox processes. *Scand J Stat* 25:451–482
- [25] Møller J, Toftaker H (2014) Geometric anisotropic spatial point pattern analysis and Cox processes. *Scand J Stat* 41:414–435
- [26] Møller J, Waagepetersen RP (2004) Statistical Inference and Simulation for Spatial Point Processes London. Chapman & Hall, Boca Raton
- [27] Ogata Y, Katsura K (1988) Likelihood analysis of spatial inhomogeneity for marked point patterns. *Ann Inst Stat Math* 40:29–39
- [28] Panaretos VM, Tavakoli S (2013) Fourier analysis of stationary time series in function space. *Ann Statist* 41:568–603
- [29] Rathbun SL, Cressie N (1994) A space-time survival point process for a longleaf pine forest in Southern Georgia. *J Am Statist Ass* 89:1164–1174
- [30] Ruiz-Medina MD (2011) Spatial autorregressive and moving average Hilbertian processes. *J Multiv Anal* 102:292–305
- [31] Ruiz-Medina MD (2012) Spatial functional prediction from Spatial Autoregressive Hilbertian Processes. *Environmetrics* 23:119– 128
- [32] Serra L, Saez M, Mateu J, Varga D, Juan P, Díaz-Ávalos C, Rue H (2014) Spatio-temporal log-Gaussian Cox processes for modelling wildfire occurrence: the case of Catalonia 1994–2008. *Environ Ecol Stat* 21:531–563
- [33] Simpson D, Illian JB, Lindgren F, Sorbye SH, Rue H (2016) Going off grid: computationally efficient inference for log-Gaussian Cox processes. *Biometrika* 103:49–70
- [34] Stoyan D, Kendall WS, Mecke J (1995) Stochastic geometry and its applications. Wiley, Chichester
- [35] Torres A, Frías MP, Ruiz-Medina MD (2016) Log-Gaussian Cox processes in infinite-dimensional spaces. *Theor Prob Math Stat* 95:157–177
- [36] Triebel H (1978) Interpolation Theory, Function Spaces, Differential Operators North-Holland, Amsterdam

- [37] Waagepetersen R, Guan Y (2009) Two-step estimation for inhomogeneous spatial point processes. *J R Statist Soc B* 71:685–702
- [38] Waagepetersen R, Guan DY, Jalilian A, Mateu J (2016) Analysis of multi-species point patterns by using multivariate log-Gaussian Cox processes. *J R Statist Soc C* 65:77–96
- [39] Wu S, Müller HG, Zhang Z (2013) Functional data analysis for point processes with rare events. *Stat Sin* 23:1–23
- [40] Yue YR, Loh JM (2013) Bayesian nonparametric estimation of pair correlation function for inhomogeneous spatial point processes. *J Nonparametr Stat* 25:463–474